INFLUENCE OF VOIDS ON WATER UPTAKE IN POLYMER PANEL

by

Fatmaelzahraa Abdelmola

A Dissertation Submitted to the Faculty of

College of Engineering and Computer Science

In Partial Fulfillment of the Requirements for the Degree of

Doctor of Philosophy

Florida Atlantic University

Boca Raton, FL

December 2018

INFLUENCE OF VOIDS ON WATER UPTAKE IN POLYMER PANELS

by

Fatmaelzahraa Abdelmola

This dissertation was prepared under the direction of the candidate's dissertation advisor, Dr. Leif A. Carlsson, Department of Ocean and Mechanical Engineering, and has been approved by all members of the supervisory committee. It was submitted to the faculty of the college of Engineering and Computer Science and was accepted in partial fulfillment of the requirements for the degree of Doctor of Philosophy.

SUPERVISORY COMMITTEE:

Leif A. Carlsson, Ph.D.
Dissertation Advisor

Javad Hashemi, Ph.D.

Hassan Mahfuz, Ph.D.

Sarah E. Du, Ph.D.

Javad Hashemi, Ph.D.
Chair, Department of Ocean and Mechanical Engineering

Stella N. Batalama, Ph.D.
Dean, College of Engineering and Computer Science

Khaled Sobhan, Ph.D.
Interim Dean, Graduate College

November 20, 2018
Date

ACKNOWLEDGEMENTS

Support for this project has been provided by the Ocean and Engineering Department (OME) and National Science Foundation (NSF) Grant No. 1562062. This support is gratefully appreciated. I would like to express sincere thanks to my Dissertation advisor, Dr. Leif .A. Carlsson, Department of Ocean and Mechanical Engineering, for guidance, continuous encouragement, and patience throughout this Ph.D. project. I would like to give a special thanks to my advisory committee members: Dr. Hassan Mahfuz, Department of Ocean and Mechanical Engineering. He kindly shared his DSC instrument, and provided continuous motivation and technical support. Dr. Javad Hashemi, Department of Ocean and Mechanical Engineering, provided financial support through the teaching assistantship (TA), and Dr. Sarah Du, Department of Ocean and Mechanical Engineering, provided useful comments. We thank Dr. Mahmoud Madani for his assistance in DMA measurements. We are also grateful for the assistance by Anthony La Vigne for help with design and manufacture of the sample holder and mold. I would like to thank Momentive Co. for donation of resin and hardener. I would also like to give thanks to my husband (Ahmed), my kids (Haitham, Rawan and Kareem) and my parents, sister, and brothers.

ABSTRACT

Author:	Fatmaelzahraa Abdelmola
Title:	Influence of Voids on Water Uptake in Polymer Panels
Institution:	Florida Atlantic University
Dissertation Advisor:	Dr. Leif A. Carlsson
Degree:	Doctor of Philosophy
Year:	2018

The influence of voids on the moisture uptake of epoxy has been studied. Specimens with void contents from 0 to about 50% were prepared. Void geometry and content were analyzed using microscopy and density methods. Void containing dry samples were characterized by Differential Scanning Calorimetry and Dynamic-Mechanical Analysis which verified consistency of chemistry of the epoxy network. The moisture uptake of specimens immersed in distilled water at 40 °C was monitored. The rate of absorption and saturation moisture content increased with increasing void content. The moisture uptake of void-free and void containing specimens was non-Fickian. The Langmuir model provided good fits to the experimental results for specimens with low to medium void content, although the moisture uptake of the high void content specimens showed substantial deviations from the Langmuir diffusion model. The moisture diffusivity agreed reasonably with predications from the Maxwell inclusion model over a range of void contents from 0 to 50%.

The state of sorbed water was examined using mass balance calculations and DSC analysis. Only 6-8% of the void volume is occupied by water at saturation. Absorbed water may be classified as free and bound water. For void-free specimens, only bound water was found. The medium and high void content specimens contained water in three states: free water, freezable bound water, and non-freezable bound water. The DSC results show that the proportions of free water and freezable bound water increase with increasing void content, while the content of non-freezable bound water decreased. Moisture induced swelling decreased with increasing void content. The swelling is attributed to the content of non-freezable bound water.

INFLUENCE OF VOIDS ON WATER UPTAKE IN POLYMER PANELS

LIST OF TABLES

LIST OF FIGURES

1 INTRODUCTION

The low density of plastics compared to traditional materials such as metals and ceramics, and the opportunities of easy manufacture and tailoring properties make plastics attractive materials in many applications, Osswald and Menges (2003). Polymers consist of large chain-like molecules (macromolecules) with a large number of repeating units in the chain. The polymer chain is flexible due to relative unconstrained rotation around single covalent bonds. The chains connect to each other by weak van der Waals forces. The molecular structure and weak inter-chain bonding of thermoplastic polymers allow a large variety of processing methods at relatively low temperatures. In thermoset polymers, molecules in the chains connect by covalent bonds, called cross-links. Thermosets have low viscosity prior to cure, but must be molded before cross-links are formed.

1.1 Moisture Uptake by Polymers

Polymers are used in numerous applications, such for example as containers for water-based liquids and matrix materials for high performance fiber-reinforced composites. The durability of the material exposed to moisture or water is an important factor for long-term applications. Many researchers have identified that the ingress of water in polymers leads to degradation of the material, such as plasticization, swelling, and reduced glass transition temperature and modulus. The mechanism of moisture uptake in polymeric resin materials without voids has been well documented and is commonly treated as diffusion described

by Fick's law, Springer (1981) and Crank (1975). Fickian diffusion is driven by concentration gradient where water molecules flow from regions of high concentration to regions of low concentration.

Sorbed water in polymers may be classified as free and bound water, Nakamura et al. (1983), Hatakeyama et al. (1988) and Trautschold (2016). Free water is the absorbed water that behaves similar to normal water, i.e. it forms a crystalline solid (freezes) and melts at a specific temperature. Free water is usually found in micro-voids and possibly in macroscopic void cavities. Bound water is absorbed water molecules that chemically attach to the polymer chain bonds with hydrogen bonds. As will be further discussed, bound water may be further classified as non-freezable bound water and freezable bound water. Free water and freezable bound water are found only at high moisture contents. It has been pointed out that bound water is responsible for volume increase (swelling) of polymers, Xiao et al. (1997).

Voids are cavities in a material introduced accidently but sometimes by purpose. Figure 1.1 presents a cross section view of the void containing polymer where the voids are indicated by black circles. Undesired voids typically form in polymers by air entrapped in the material during liquid processing. Undesired voids may also develop in a thermoset polymer during liquid resin processing due to gas formation from chemical reactions between resin and catalyst.

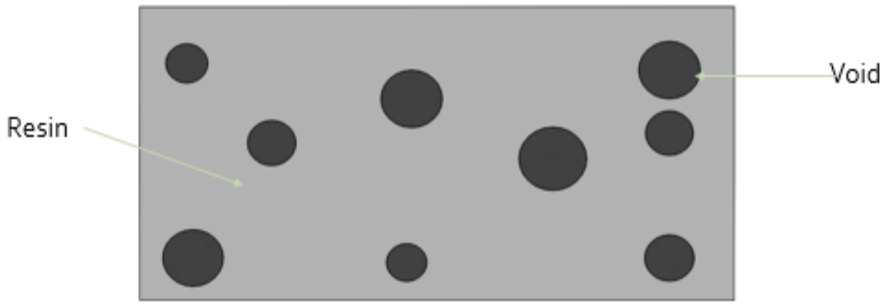

Figure 1.1 Schematic of voids in polymer resin.

For polymers containing voids, the moisture uptake has received little attention. The inhomogeneity on a microstructural level provided by voids and the various states of sorbed water (free and bound) present difficulties in the analysis of the moisture transport. In general the water transport in a void containing polymer cannot be considered as a single-phase process as in Fickian diffusion. Moisture will diffuse from the external boundaries of the specimen and when water molecules reach an internal cavity (void) they will diffuse into the void cavity. The vapor pressure inside the void will increase. If pressure builds up sufficiently, the water vapor may condense and form liquid water, He and Fan (2007).

He and Fan (2007) investigated moisture absorption-desorption in a thin layer of a bismaleimide-triazine (BT) resin/glass fiber laminate with voids. Their results suggest that the voids will eventually fill up with water due condensation due to increased vapor pressure.

1.2 Problem Statement

The primary objective of this research is to study the mechanism of water uptake in void-free and void containing specimens. The study work includes experimental testing as well as analytical modeling.

1.3 Research Objectives

The major objectives of this dissertation project are to experimentally determine water uptake characteristics of void-free and void containing polymers, and model the moisture uptake process using macroscopic and micromechanics models. These objectives are achieved by:

- Selection of a host polymer that can be modified by void-forming chemicals without affecting the chemistry of the host polymer.
- Develop processing methods to achieve void-free and void containing specimens with a range of void contents from 0 to about 50%.
- Verify consistency of chemistry of the host polymer by Differential Scanning Calorimetry (DSC) and Dynamic Mechanical Analysis (DMA) of dry void-free and void containing specimens.
- Examine microstructure and void size of void-free and void containing specimens by optical microscopy, image analysis, and density measurement.
- Determine moisture uptake (weight gain) versus time for void-free and void containing specimens immersed in distilled water at 40 °C.
- Analyze the state of water in the moisture aged void-free and void containing specimens by DSC analysis.
- Measurement and analysis of swelling strain.
- Modeling of moisture up-take using single phase and two-phase diffusion models (Fickian and Langmuir).
- Modeling of moisture uptake using mass balance and micromechanics models.

1.4 **Outline of the Research**

Epoxy resin “Epon 828” is selected as the base polymer resin. This resin absorbs moderate amounts of water, and has been widely characterized in the literature. Specimens with void contents ranging from 0 to about 50% prepared using two foaming agents added to the liquid epoxy resin are examined. Differential scanning calorimetry (DSC) and dynamic mechanical analysis (DMA) characterization of dry void-free and void containing specimens is conducted to verify the consistency of the resin chemistry after adding the foaming agents. The void shape, size and void content are determined and analyzed by optical microscopy and image analysis. In addition, density measurements are performed to determine void content. The moisture uptake vs. time for the void-free and void containing specimens immersed in distilled water at 40 °C is determined using gravimetric method (weight gain). The state of water in the moisture aged void-free and void containing specimens is analyzed by DSC. The moisture swelling strain for the void-free and void containing specimens is measured and correlated with the state of water results from the DSC anylsis. The moisture uptake for the void-free and void containing specimens is modeled using diffusion models (Fickian and Langmuir). The saturation moisture content for specimens with voids is also modeled using mass balance analysis. The diffusivity of void containing specimens is analyzed using a micromechanics model.

2 BACKGROUND

2.1 Polymers

Polymers are materials made from large organic molecules consisting of monomers (smaller molecules) arranged in a chain structure. Polymers are mainly divided into thermoplastics and thermosets. Polymers may be classified based on their molecular structure. The chains may be connected only with weak van der Waals forces, or they may be cross linked where the chains are connected by covalent bonds. The first type of polymer is called thermoplastic and the second thermoset.

When thermoplastics are heated above a certain temperature, the weak van der Waals bonds are broken and chains may be able to slide relative to each other which results in flow. This is the basis for melt-processing of thermoplastics. Examples of thermoplastics are polypropylene, polyvinyl chloride, and nylon. Thermosets have polymer chain molecules connected by covalently bonded chain (cross-links). Thermosets solidify by an irreversible chemical reaction, called cure. During cure, small molecules combine to form macromolecular networks. Thermosets do not return to a liquid when heated, because the cross-links restrict flow. Examples of thermosets materials are epoxy, phenolics, and unsaturated polyster.

Thermosets and many thermoplastics have an amorphous structure with chains arranged in a random molecular structure. Amorphous polymers are solid (glass-like) below the glass transition temperature, T_g. If they heated above T_g, they transition into a rubbery state.

2.2 Voids in Polymers

Voids are isolated empty cavities in materials. Voids may form in thermoset polymers due to evaporation of moisture entrapped in the resin during liquid resin processing or gas formation from the chemical reaction between a thermoset resin and curing agent. Voids degrade the mechanical properties of polymers as they create stress concentration. Voids may also elevate water uptake of polymers.

In many cases, voids in polymers are desired, such as in polymer foams as they are provide a bulky light weight material. Syntactic foams are made by mixing hollow spheres called "microballoons" in a liquid thermoset polymer resin. More commonly, however, polymer foams are made by adding a foaming agent that evolves gas upon heating of the liquid resin. Examples are polyutherane, polyvinyl chloride (PVC), polystyrene, and polyimide foams. Figure 2.1 shows a micrograph of PVC foam, Poapongsakorn and Carlsson (2013). The void content in PVC foams is very large, 91 to 98%.

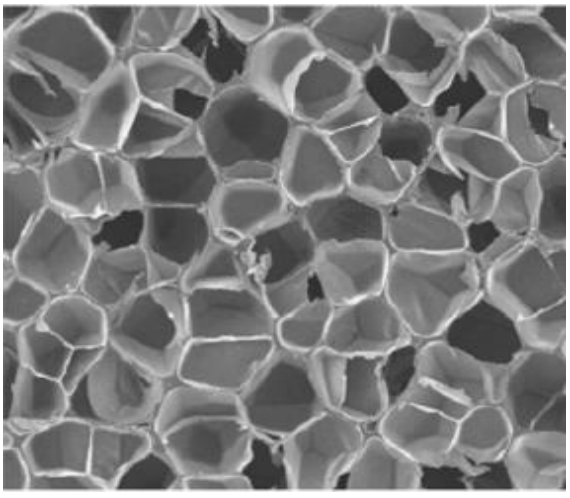

Figure 2.1 SEM micrographs of PVC foam, Poapongsakorn and Carlsson (2013)

An example of an epoxy polymer with voids (desired voids) is shown in Figure 2.2, Manfredi et al. (2006). The size of the voids ranges from 20-30 μm.

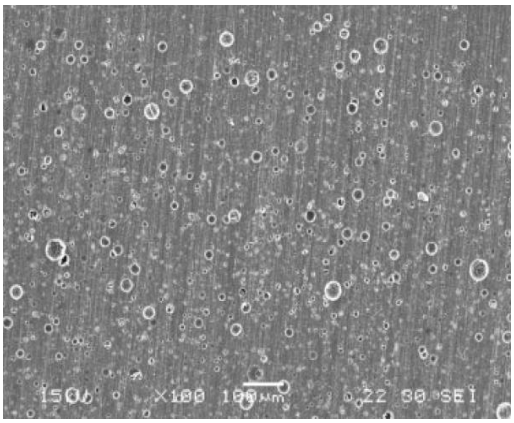

Figure 2.2 SEM micrograph of voids in an epoxy specimen, Manfredi et al. (2006)

It is well-known that voids have a negative effect on the strength of polymers and composite materials as they cause stress concentration. In addition, water uptake has been found to be amplified by the presence of voids, Thomason (1995b) and Manfredi et al. (2006).

2.3 Microstructural characterization of a polymer with voids

For polymers containing voids it is of the interest to determine their size, geometry (shape) and volume. Different techniques are used to characterize voids in polymer resins such as: optical microscopy, scanning electronic microscopy (SEM), micro computed tomography (μCT), and density method. The void volume fraction $\mathbf{v_v}$ is defined as:

$$\mathbf{v_v} = \frac{\mathbf{V_v}}{\mathbf{V}} \tag{2.1}$$

where V_v is the total volume of voids in a specimen, and V is the macroscopic volume of the specimen. $\mathbf{v_v}$ is commonly called "void content".

2.3.1 Microscopy

A common method used to characterize voids in materials is to cut a sample, sand and polish the cross section which will be examined in an optical or scanning electron microscope (SEM). Determination of the 3D distribution of voids using microscopy requires observation of several cross sections, Little el al. (2012).

Void area fraction determined from a micrograph is commonly used to estimate the void volume fraction, Kuo and Frost (1996), and Hilliard (1968). A direct area-to-volume conversion assumes the voids are close to spherical in shape and distributed randomly inside the specimen, Papthanasiou and Guell (1997).

2.3.2 Image Analysis

Image analysis is a computer based method developed to extract information from a digital image using image processing techniques and utilized as a fundamental tool to recognize, differentiate, and quantify diverse types of grayscale images and color images, Mendoza and Lu (2015). The digital form of an image is a set of pixels which can be assigned a shade of gray or color. To get a meaningful results from Image analysis, the image has to be calibrated.

Image analysis are used to measure area by particles counting. The ImageJ software, Rasband (1997), used here is an image processing software used for quantitative analysis of materials microstructure. Image analysis techniques was conducted earlier by Carnachan el al. (2006) to examine void size distribution in a polymer (polyHIPE).

2.3.3 Density

Density measurement is a common method to determine the overall void content in a sample, Thomason (1995a), and Santulli et al. (2002). The density (ρ) is defined as mass

of the specimen (m) divided by its volume (V). The ASTM standard D2734-09, (2008) defines the void content as,

$$v_v = 1 - \frac{\rho}{\rho_m} \tag{2.2}$$

where ρ and ρ_m are the densities of the void containing specimen, and the solid void-free material (reference).

The mass of the specimen is determined by weighing. The specimen volume may be calculated from the specimen dimensions using e.g. digital caliper and micrometer. Another method to determine the volume is to use Archimedes method, Hughes (2005). This method utilizes weighing in air and hydrostatic weighing (underwater weighing). The Archimedes method obviously does not work well for materials with density less than water (ρ_w = 1 g/cm^3) since the specimen will float on the surface of water.

2.3.3.1 Micro-Computed Tomography (µCT)

Micro-Computed Tomography (µCT) is a method where a specimen is illuminated with x-rays and a planar x-ray detector collects a magnified projection image. Several projection images are acquired by rotating specimen. A computer code is used to combine such cross section images and construct a 3D image of the damage, Little et al. (2012). The µCT has recently been introduced as powerful non-destructive method for detailed detection of damage in a composite material, Wright et al. (2008).

Image analysis of a µCT image of a specimen containing voids provides overall void content, number of voids in a specimen and size and shape of voids without slicing the sample, Little et al. (2012). µCT is a technique for analysis of void morphology of polymer composite materials and has a resolution of about 7µm.

Figure 2.3 shows an example of µCT image of the void structure in a glass fiber/epoxy cross-ply composite laminate.

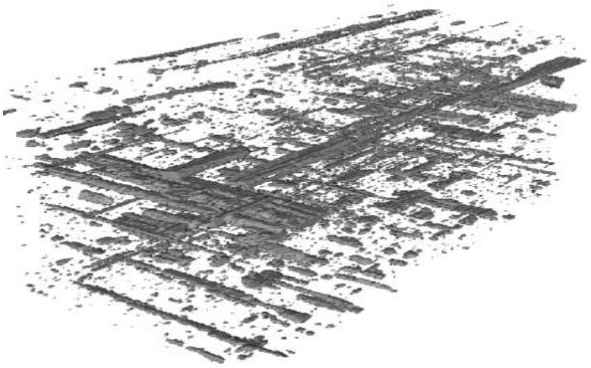

Figure 2.3 3D µCT image of a glass fiber/epoxy cross-ply composite laminate, Little et al. (2012)

Large elongated voids following the fibers are observed in the image besides isolated voids scattered in the matrix, see Fig. 2.3. The µCT technique, however, is limited to small sample dimensions (< 20 mm) and requires long scanning times because of the large amount of data collected.

2.3.4 Differential Scanning Calorimetry (DSC)

DSC is a thermal analysis technique used to characterize thermal transitions in a polymer by measuring the thermal energy absorbed or released, Aklonis and MacKnight (1983). DSC has been used to characterize major transitions such as melting and glass transition, Mutlur (2004). An endothermic peak is observed when the polymer absorbs heat, such as when the material melts. An exothermic peak is recorded when the polymer releases heat. DSC measures the heat absorbed or released by a polymer sample and a reference sample as a function of time or temperature under heating, cooling, or isothermal conditions, Hatakeyama and Quinn (1999).

Figure 2.4 shows a schematic of DSC curve for a polymer. Glass transition is a major thermal transition observed when an amorphous polymer transitions from a glassy to a rubbery state. The glass transition temperature (T_g) is detected as a drop (discontinuity) in the heat flow curve. The exothermic peak at a temperature T_c occurs when the polymer sample is not fully cured as it releases heat during thermosets curing. An endothermic peak is displayed when the polymer sample absorbs heat, such as melting, at a temperature (T_m). Notice, however, that amorphous polymers do not physically melt.

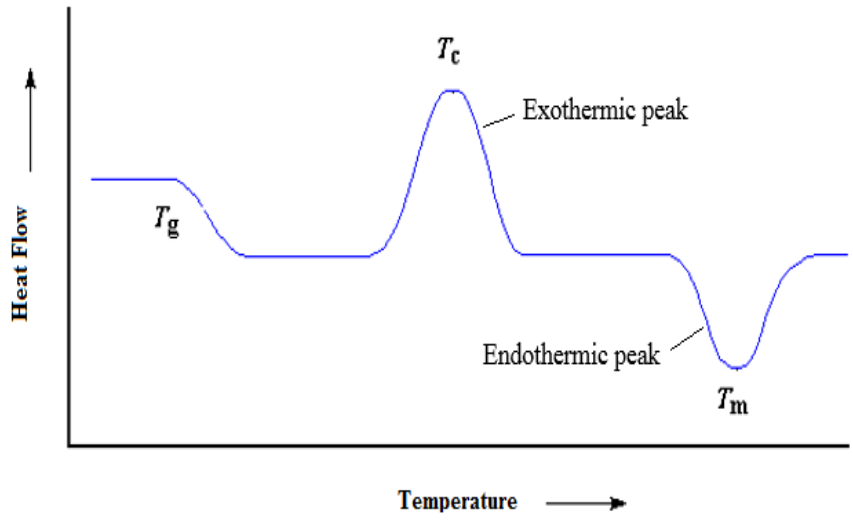

Figure 2.4 Typical DSC curve thermal transitions are T_g, T_c and T_m

2.3.5 Dynamic-Mechanical Analysis (DMA)

DMA is a technique in which a polymer specimen is subject to dynamic (cyclic) loading. In this method, the stress and strain signals are analyzed to determine the complex modulus E*, and the storage and loss moduli (E' and E''), Foreman (1997).

The storage modulus E' represents solid-like elastic behavior, while the loss modulus E" indicates viscous damping. The ratio of loss modulus to storage modulus is defined as the loss tangent tan δ, Aklonis and MacKnight (1983),

$$\tan \delta = \frac{E''}{E'} \tag{2.3}$$

Jordan et al. (2008) determined the storage and loss moduli (E' and E") of epoxy specimens by DMA test. They performed DMA tests over a range of temperatures from -125 to 200 °C at frequencies of 1, 10, 100 Hz. Figure 2.5 displays E' and E" vs. temperature for Epon 826/DEA.

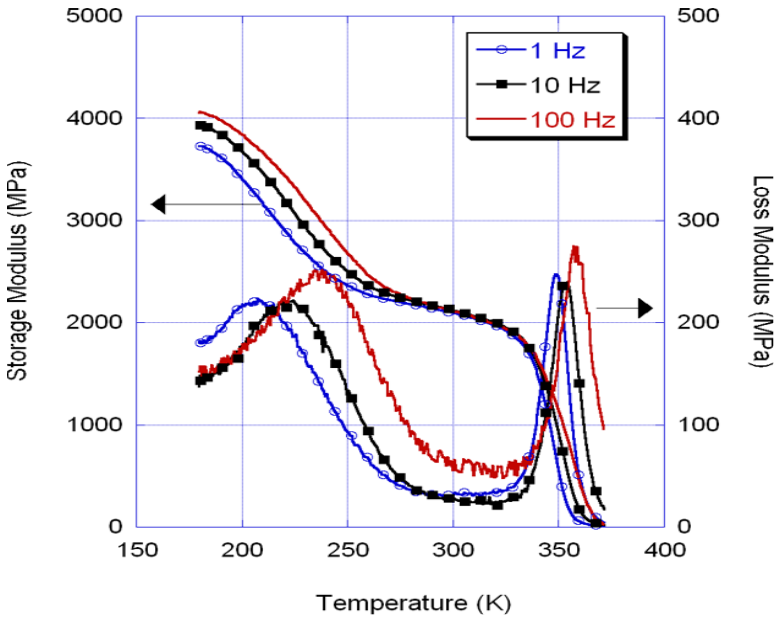

Figure 2.5 Storage and loss moduli of Epon 826/DEA specimens, Jordan et al. (2008)

It is noted that the storage modulus drops from about 4 GPa in the glassy region to 2 GPa in the rubbery region. The glass transition temperature of Epon 828/DEA is around 370 K (100 °C) as determined from the second peak in the loss modulus curve. Notice that T_g increases with increasing frequency.

Grave et al. (1998) performed DMA test on dry epoxy samples and epoxy samples after being immersed in water for 21 days. DMA was conducted at a frequency of 1 Hz, over a range of temperatures from 0 to 150 °C. Figure 2.7 shows E' and tan δ plotted versus temperature. Moisture uptake by the epoxy resin reduced the modulus E' in the glassy region and the glass transition temperature T_g by 10 °C, see Fig. 2.6. Notice that the scale of the storage modulus E' is obviously off but the trends are correct.

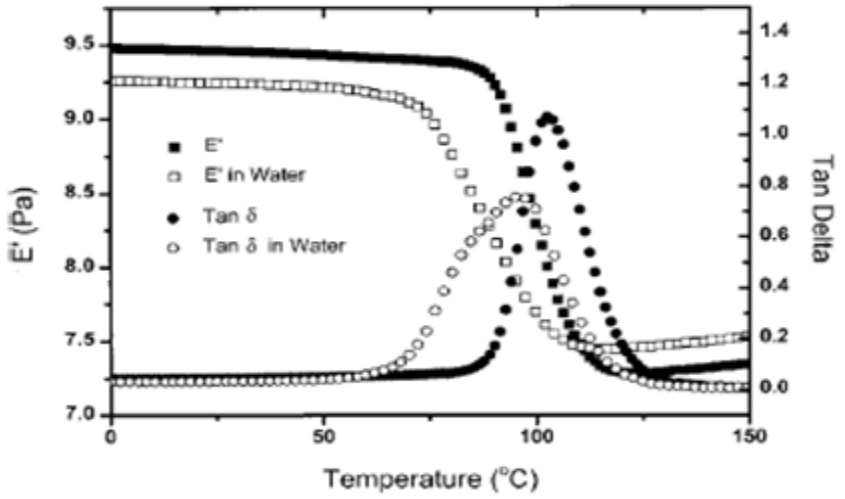

Figure 2.6 DMA results for dry and wet epoxy samples, Grave et al. (1998)

2.4 Water Uptake in Polymers

Polymers absorb water but are typically not soluble in water. Water absorption depends on the polymer chemical structure, the surrounding environment (humid air or liquid water), and temperature, Vesely (2008), and Trautschold (2016). Numerous studies show that the ingress water in polymers tends to degrade the material, manifested in reduced glass transition temperature and modulus, e.g. De'Nève and Shanahan (1993), Alamri and Low (2012), Nogueira et al. (2001), Deroiné et al. (2014) and Zhou and Lucas (1999).

Many experimental methods are used to characterize the water uptake in polymers. The most common method is gravimetric determination of the added mass, Weitsman (1998). Methods such as nuclear magnetic resonance, differential scanning calorimetry, infrared Fourier transform spectroscopy, and dielectric spectroscopy have also been used to monitor water uptake, Vesely (2006).

Gravimetric method is a simple and accurate method to measure moisture uptake. In this test, a specimen is exposed to humid air or immersed in water, and the amount (mass) of water absorbed is measured as a function of time. The moisture content is calculated from the weight gain as follows:

$$M(t) = \frac{m(t) - m_0}{m_0} \tag{2.4}$$

where m(t) is the mass of the polymer after absorbing moisture for a specified time (t) and m_0 is the mass of the dry polymer.

The moisture uptake in polymeric resins without voids has been well documented. Moisture absorption experiments on epoxy panels (DGEBA/DGEBF) immersed in deionized water at temperatures 20, 40, and 65 °C were conducted for 14 months by Perrin et al. (2009). Figure 2.7 shows the moisture content is plotted vs. $\sqrt{t}/h$, where h is the specimen thickness. The moisture uptake is initially linear vs. $\sqrt{t}/h$ and approaches saturation asymptotically. The rate of absorption and the saturation moisture content (M_∞) increase with increased water temperature.

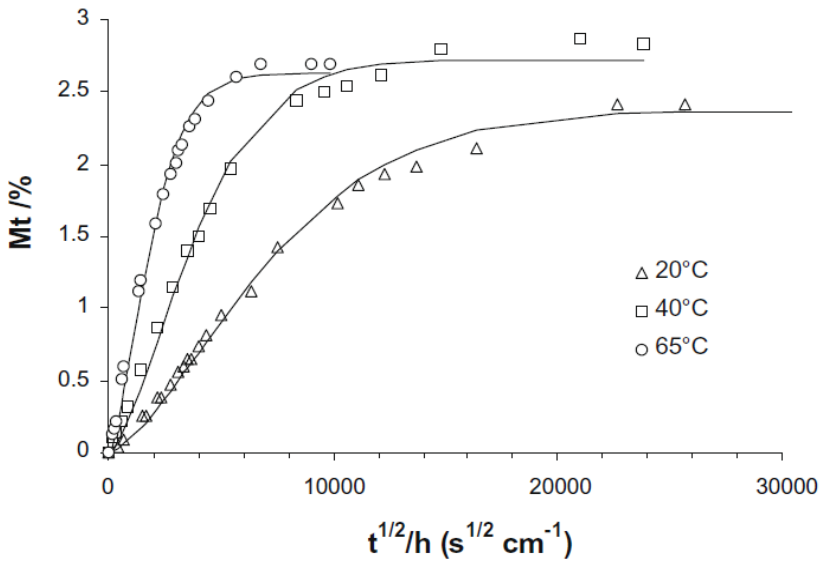

Figure 2.7 Moisture uptake of epoxy (DGEBA/DGEBF) immersed in water at 20, 40, and 65 °C water temperatures, Perrin et al. (2009).

The moisture uptake in void containing polymers, however, has received much less attention, Lopez et al. (2016), examined moisture uptake by a semicrystalline fluropolymer immersed in water, see Fig. 2.8. The moisture uptake increases with increasing void content (porosity). The reference sample (void-free) reached saturation at a small moisture content at shorter times. The void containing samples absorb much more water over long times compared to the reference void-free sample.

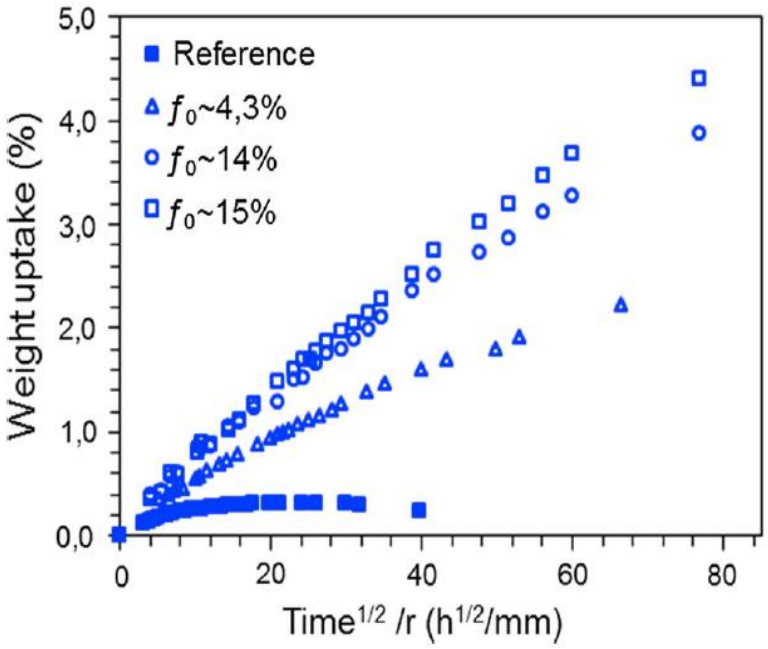

Figure 2.8 Water uptake by fluoropolymer samples with different void contents (f_0) in water at 40 ºC, Lopez et al. (2016).

Li and Weitsman (2004) immersed closed cell PVC foam in sea water. They found the water uptake mechanism started with water molecules filling the open cells at the foam surface which was followed by a slow process where water molecules diffused through the cell walls prior to entering the neighboring cells. After long term immersion, however they found the interior part of the PVC foam panel remained dry. Earl and Shenoi (2004) similarly examined the moisture uptake in closed-cell PVC foams immersed in water. Similar to Li and Weitsman (2004), they found that the moisture uptake occurs in multi-stage process where water molecules diffuse through the cell walls into neighboring foam cells.

The influence of voids on water uptake in glass/epoxy composite materials was examined by Thomason (1995b). He found that voids greatly elevate moisture uptake and his results indicate that the voids may contain water.

2.4.1 Free Volume Theory for Water Absorption

Polymers contain free volume which is molecular size empty space (voids) in the amorphous regions between polymer chains and near the chain ends, Young and Lovell (2011). Free volume is an important quantity that may explain several phenomena observed in amorphous polymers, Adamson (1980), Aklonis and MacKnight (1983).

The free volume is minimum when the temperature is below the glass transition temperature, typically 2.5% of the total volume for an amorphous polymer, Budd et al. (2005). When the polymer is heated, the free volume expands allowing more space for motions of chain segments which causes the material to transition from a glassy to rubbery state. The change in volume is commonly measured by the specific volume, i.e. volume divided by mass (cm^3/g). The upper solid curve in Figure 2.9 shows specific volume vs. temperature for PMMA, Rusch (1968).

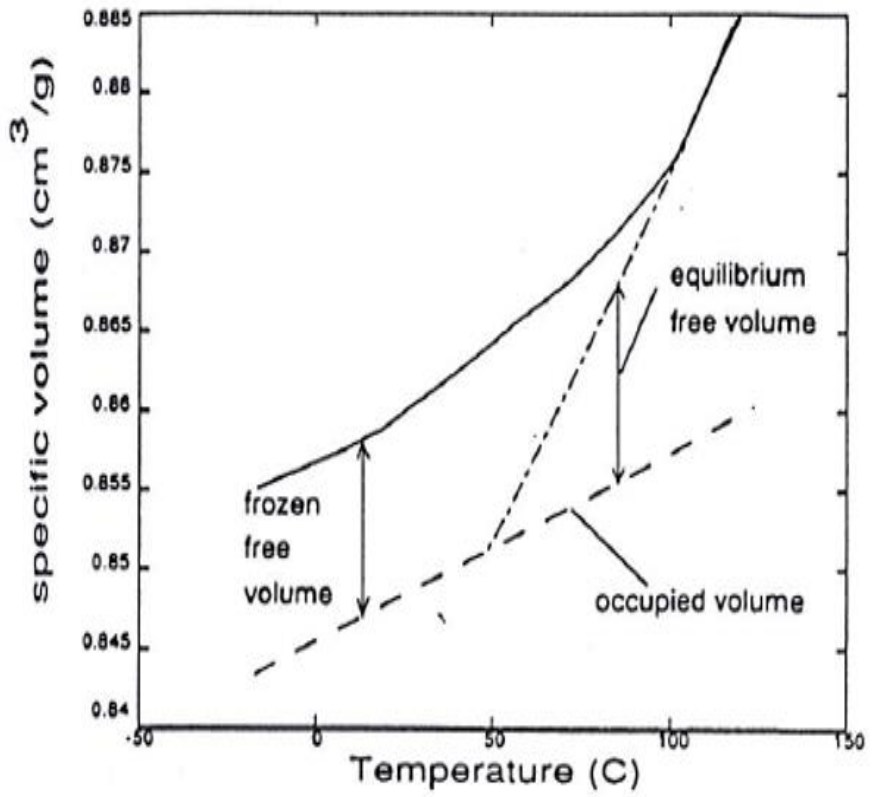

Figure 2.9 Specific volume vs. temperature for PMMA, Rusch (1968).

The lower dotted line in Fig. 2.9 indicates the volume occupied by the PMMA molecules. The difference between the upper solid curve and the lower dotted line is the free volume. At the glass transition temperature T_g (about 100 ºC), the specific volume increases with a higher rate.

2.4.2 Moisture Swelling

Moisture swelling may be considered as a volumetric strain defined as the relative volume increase upon water saturation, Adamson (1980), and González et al. (2012),

$$\frac{\Delta V}{V_0} = \frac{V_\infty - V_0}{V_0} \tag{2.5}$$

where V_0 and V_∞ are the volumes of the dry and saturated specimen.

The added volume of water absorbed by the polymer sample is expected to contribute to the volume increase. The added volume of water absorbed can be calculated by dividing the mass of water absorbed by the density of the polymer specimen. If all the absorbed volume of water contributes to swelling, the swelling strain $\Delta V/V_0$, should be equal to the relative increase of water volume, $\Delta V_w/V_0$. In reality, the swelling strain tends to fall below this ratio.

Figure 2.10 shows the moisture swelling vs. the added volume of water absorbed in 3501 epoxy specimen, Adamson (1980). The dashed line is the moisture swelling (the added volume) when the absorbed water is fully converted to volume. Adamson (1980) found that the moisture swelling (solid line) falls below the volume of water absorbed (dashed line). He explained that part of the absorbed water molecules enter in the polymer free volume which does not cause moisture swelling.

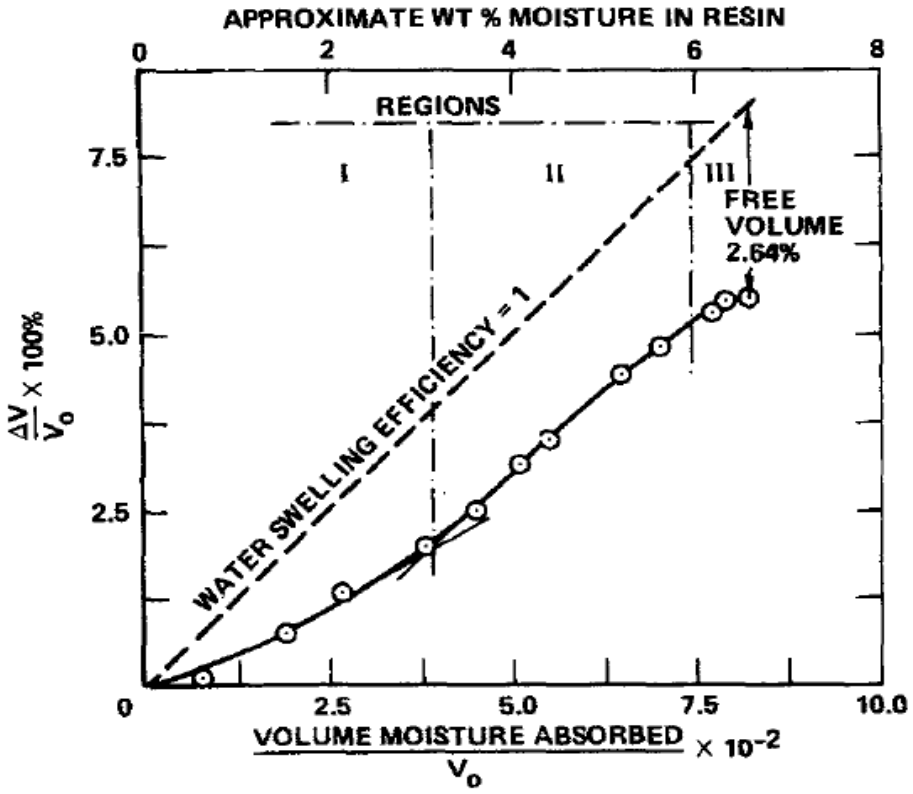

Figure 2.10 Swelling vs. volume of water absorbed for 3501 epoxy specimen immersed at 74 °C, Adamson (1980).

2.4.3 State of Sorbed Water in Polymers

Differential scanning calorimetry (DSC) analysis, Section 2.4, was applied to polymers after they were allowed to absorb water, Nakamura et al. (1981) and (1983). They prepared water-aged polyhydroxystyrene (PpHS) specimens with moisture contents ranging from 7.8 to 26.3 %.

Figure 2.11 shows schematic DSC curves for a polymer specimen containing sorbed water, Nakamura (1981). When the specimen is cooled from RT to -80 °C, two exothermic peaks are observed at temperatures of about -20 °C and -40 °C. The sharp peak at -20 °C corresponds to freezing of free water which solidifies into a crystalline form different than ordinary ice which a melting/solidification temperature of 0 °C, Nakamura (1981). The

free water peak becomes more pronounced at higher moisture contents. The smaller exothermic peak at -40 °C is attributed to the freezing of a fraction of the bound water (freezable bound water). When the specimen is heated back to RT (top curve in Fig. 2.11), a sharp endothermic peak is found which represents melting of the freezable water, i.e. free water and freezable bound water. This peak occurs at about 0 °C, i.e. as for ordinary ice.

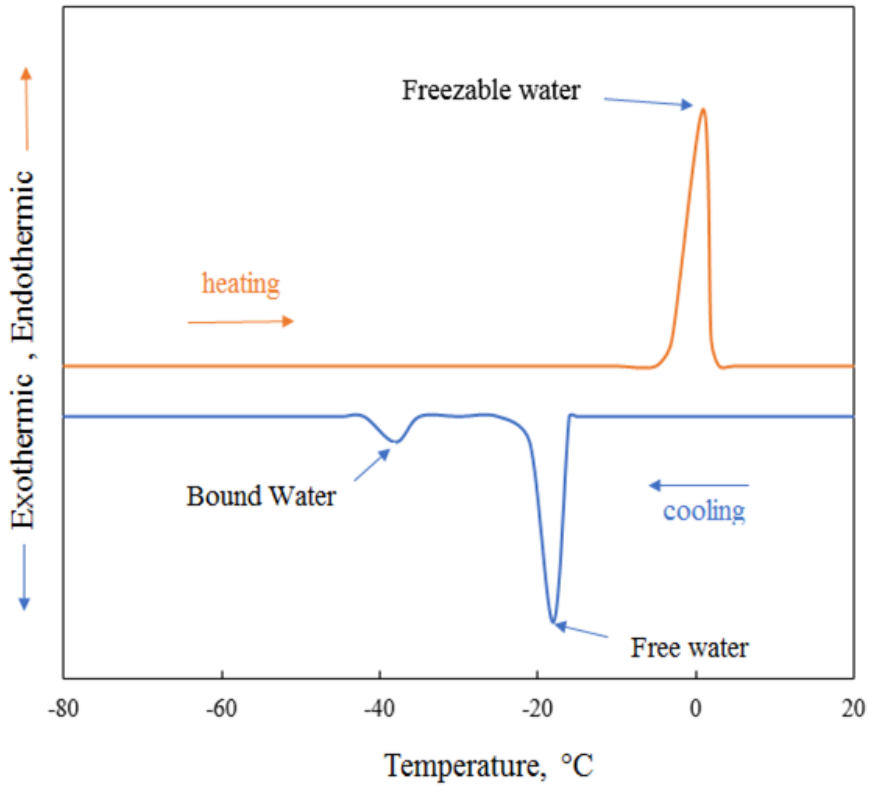

Figure 2.11 Schematic DSC curves cooling and heating of water sorbed in polymers, Nakamura (1981).

Ping et al. (2001) similarly conducted DSC studies to examine the state of the water sorbed in poly(vinyl alcohol) (PVA) and poly(ethylene)-g-acrylic acid. After exposure to humid air, sorbed water molecules bond to hydrophilic sites to form bound water. Some of the

sorbed water was identified as freezable bound water. At higher water contents, free water was detected.

Other methods such a Nuclear Magnetic Resonance (NMR), and Fourier Transform Infrared (FTIR) have been found useful to identify the state of sorbed water, Zhou and Lucas (1999), Maxwell and Pethrick (1983), Xiao (1997), and Ping et al. (2001). Furthermore, Maxwell and Pethrick (1983) studied the dielectric properties of dry and water aged epoxy samples at different temperatures. Tests were conducted at fixed and variable frequency over a range of temperatures to measure the dielectric permittivity of the saturated epoxy samples. The dielectric permittivity was higher for saturated water epoxy samples than for dry epoxy samples which was attributed to the existence of free water in the epoxy samples. They also found that bound water in the epoxy chain decreases the dielectric permittivity.

2.4.4 Quantitative Analysis of State of Water

The weight percent of freezable water can be calculated from the endothermic peak observed close to 0 °C in the DSC heating curve (Fig. 2.11), Hodge (1996),

$$W_{fz} = \left(\frac{Q_{fz}}{\Delta H_w^h}\right) 100 \tag{2.6}$$

where Q_{fz} is the area under the endothermic peak, ΔH_w^h is the enthalpy of ice-water transition of pure water (293.6 J/g), Hodge (1996). The weight percent of non-freezable bound water W_{nf} can be determined as,

$$W_{nf} = M(t) - W_{fz} \tag{2.7}$$

where M(t) is the total weight percent of absorbed water "moisture content" defined in Eq. (2.4), and W_{fz} is defined in Eq. (2.6).

The weight percent of free water can be determined from the exothermic peak at -20 °C in (Fig. 2.11) in the DSC cooling curve, Hodge (1996),

$$W_f = \left(\frac{Q_f}{\Delta H_{fu}}\right) 100 \tag{2.8}$$

where Q_f is the area under the exothermic peak, and ΔH_{fu} is the enthalpy of fusion for the water-ice transition (ΔH_{fu} = 219.6 J/g), Hodge (1996).

Similarly, the weight percent of freezable bound water can be calculated from the small exothermic peak at -40 °C (Fig. 2.11) of the cooling curve obtained in the DSC analysis, Hodge (1996),

$$W_b = \left(\frac{Q_b}{\Delta H_{fu}}\right) 100 \tag{2.9}$$

where Q_b is area under the peak.

2.5 Modeling Water Uptake in Polymers

A common framework to describe the moisture sorption and desorption in polymers is Fick's laws based on moisture transport by diffusion, Crank (1979) and Springer (1981). Diffusion is a molecular process where the moisture transports inside the polymer from the region of higher concentration to the lower concentration region. Fick's first law states that the flow of water molecules expressed as flux j (kg/m^2.s) is proportional to the gradient of the moisture concentration in the material, Crank (1979),

$$j = -D \text{ grad C} \tag{2.10}$$

where D is the diffusivity (m^2/s), a quantity that quantifies the rate at which the moisture is absorbed in the material. C is the concentration C = C(x, y, z, t) (kg/m^3), and ($\frac{\partial C}{\partial x} + \frac{\partial C}{\partial y} + \frac{\partial C}{\partial z}$) is the concentration gradient for the case of a 3D diffusion flow along (x, y, z) axes.

Fick's second law considers the conservation of mass. If the diffusivity D is constant, and the diffusion occurs in 3D, it is possible to express the change of concentration at a point, Crank (1979),

$$\frac{\partial C}{\partial t} = D\left(\frac{\partial^2 C}{\partial x^2} + \frac{\partial^2 C}{\partial y^2} + \frac{\partial^2 C}{\partial z^2}\right) \tag{2.11}$$

For a thin plate with the top and bottom surfaces exposed to moisture, Fig. 2.12, the diffusion may be assumed 1D, i.e. transport occurs only along the z axis, Crank (1979), Eq. (2.11) becomes,

$$\frac{\partial C}{\partial t} = D\frac{\partial^2 C}{\partial z^2} \tag{2.12}$$

where C = C (z, t).

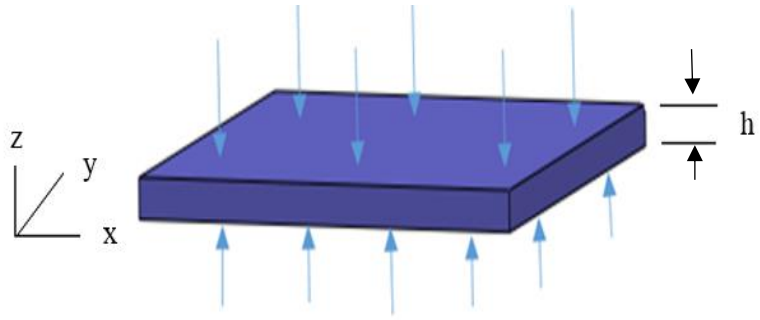

Figure 2.12 A thin plate exposed to moisture at top and bottom surfaces (z direction).

The panel is assumed to initially have a uniform moisture concentration. This may be expressed as,

$$C = C_0 \qquad 0 < z < h \qquad t \leq 0 \tag{2.13a}$$

where C_0 is the initial concentration of the moisture.

At time zero, the panel is assumed to be immersed in water. This corresponds to,

$$C = C_\infty \qquad z = 0 \text{ and } h \qquad t > 0 \tag{2.13b}$$

where C_∞ is the saturated moisture concentration.

The general solution of Eq. (2.12) under the boundary conditions (2.13) is given by Crank (1979) provides the moisture concentration C(z, t) as a function of z and time as follows,

$$\frac{C(z,t)-C_0}{C_\infty-C_0} = 1 - \frac{4}{\pi}\sum_{n=0}^{\infty}\frac{(-1)^n}{(2n+1)} exp\left[\frac{-(2n+1)^2\pi^2 Dt}{4h^2}\right]\cos\left(\frac{(2n+1)\pi z}{2h}\right) \tag{2.14}$$

If the specimen is assumed that to be initially dry ($C_0 = 0$). Equation (2.14) becomes,

$$\frac{C(z,t)}{C_\infty} = 1 - \frac{4}{\pi}\sum_{n=0}^{\infty}\frac{(-1)^n}{(2n+1)} exp\left[\frac{-(2n+1)^2\pi^2 Dt}{4h^2}\right]\cos\left(\frac{(2n+1)\pi z}{2h}\right) \tag{2.15}$$

The moisture content at time (t) is obtained by integrating the concentration over the plate thickness (h), Springer (1981),

$$M(t) = \int_0^h C(x,y,z,t)\, dxdydz \tag{2.16}$$

Integration of Eq. (2.15) yields,

$$M(t) = M_\infty\left(1 - \frac{8}{\pi^2}\sum_{n=0}^{\infty}\frac{1}{(2n+1)^2} exp\left[\frac{-(2n+1)^2\pi^2 Dt}{4h^2}\right]\right) \tag{2.17}$$

For short exposure times, Crank (1979) provides an approximate expression for the moisture content M(t),

$$M(t) = M_\infty \frac{4}{h}\sqrt{D}\sqrt{\frac{t}{\pi}} \qquad , \qquad \frac{Dt}{h^2} < 0.05 \tag{2.18}$$

For longer exposure times, the moisture content may be approximated by the 1st term (n = 0), Crank (1979),

$$M(t) = M_{\infty}\left[1 - \frac{8}{\pi^2} e^{\left(-\frac{Dt}{h^2}\pi^2\right)}\right] \quad , \quad \frac{Dt}{h^2} > 0.05 \tag{2.19}$$

The diffusivity (D) is considered as the speed by which the moisture is absorbed by a polymer. The diffusivity depends on the composition of the fluid, the moisture concentration inside the specimen, the specimen geometry, the fluid temperature, and the chemical composition of the polymer, Weitsman (2012).

The temperature dependence of diffusivity is commonly expressed by the Arrhenius equation, Weitsman (1998),

$$D = D_0 exp\left(\frac{-E}{RT}\right) \tag{2.20}$$

where D_0 is a reference diffusivity, E is the activation energy for diffusion, R is the gas constant and T is the absolute temperature (°K).

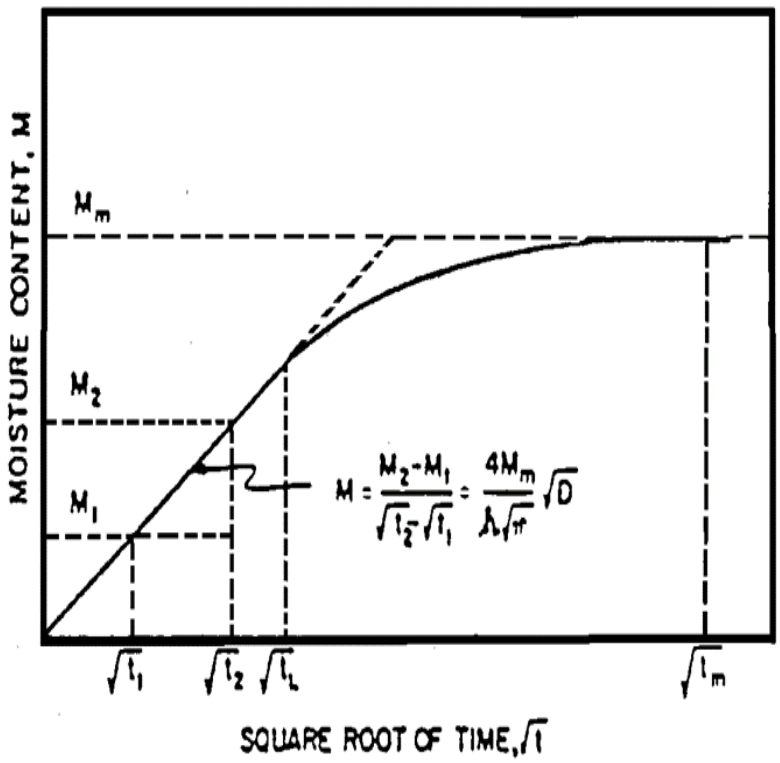

Figure 2.13 Illustration of Fickian model, Springer (1981).

Figure 2.13 shows moisture content vs. square root of time curve for the Fickian model, Springer (1981). At short times, the slope of the linear region is used to solve for the diffusivity (D) using the saturated moisture content M_m.

$$D = \left(\frac{h\sqrt{\pi}}{4M_m}\right)^2 (\text{slope})^2 \qquad (2.21)$$

2.5.1 Non-Fickian Diffusion

Non-Fickian diffusion is defined when the moisture absorption in polymers deviates from the Fickian diffusion model predictions. Weitsman (1998) discussed several such cases for polymers and polymeric composites, see Fig 2.14. The Fickian model is represented by the solid bold curve (LF). Curves (A, B, C and D) display the sorption of polymers that deviate from the Fickian diffusion model. Curves A and B are called two-stage diffusion.

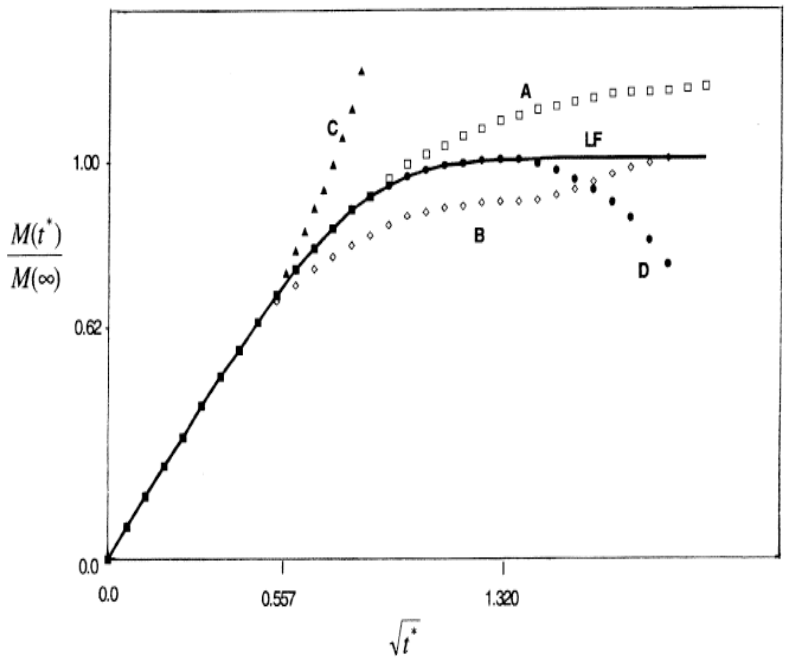

Figure 2.14 Fickian and non-Fickian model curves, Weitsman (1998).

Deviations from the Fickian diffusion model such as curve A in Fig. 2.14 were reported by Carter and Kibler (1978), who accommodated the two states of water (free and bound) and proposed a two-phase diffusion model called Langmuir model. The Carter and Kibler (1978) Langmuir type model for 1D diffusion includes four parameters D (diffusivity), M_∞ (saturation moisture content), α the probability of bound water molecules to convert into free water, and β the probability of free water molecules to change into bound water.

Bonniau and Bunsell (1981) expressed the Langmuir model in the form of a modified 1D Fickian model (Eq. 2.17) to predict the moisture content function the time,

$$M(t) = M_\infty \left[1 - \frac{\beta}{\alpha+\beta} exp(-\alpha t) - \frac{\alpha}{\alpha+\beta} \cdot \frac{8}{\pi^2} \sum_{n=0}^{\infty} \frac{1}{(2n+1)^2} exp\left(-\frac{\pi^2 Dt}{h^2} \cdot (2n+1)^2\right)\right] \quad (2.22)$$

As pointed out by Bonniau and Bunsell (1981), the Fickian two-parameter single-phase 1D diffusion model may be recovered by setting α = 1 and β = 0 in Eq. (2.22).

Carter and Kibler (1978) used the Langmuir model, Eq. (2.22), to analyze the moisture uptake of epoxy 5208 resin samples exposed to different relative humidities. Figure 2.15 shows the moisture content for the epoxy 5208 resin specimens exposed to 45.5, 75.5, 97.5, and 100 % relative humidity. They found a good fit of the Langmuir model to the experimental results using α =0.00035 day^{-1} and β = 0.0021 day^{-1} for all humidities.

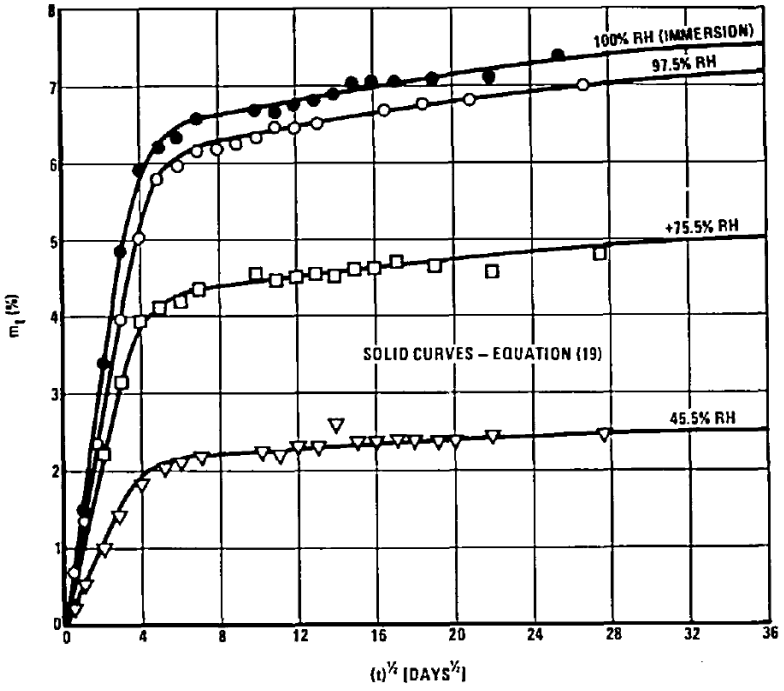

Figure 2.15 Moisture content vs. square root of days for epoxy 5206 specimens at to 45.5, 75.5, 97.5, and 100% RH. The points are experimental data and the solid lines represent Langmuir model, Carter and Kibler (1978).

Bonniau and Bunsell (1981) examined the applicability of Fickian and Langmuir models on glass /epoxy composite specimens cured with different hardeners exposed to humid air and water. They found that moisture uptake by specimens cured with diamine hardener followed Fickian diffusion, while specimens cured with dicyandiamide hardener obeyed the Langmuir model.

Glaskova et al. (2007) examined the moisture uptake in epoxy specimens (Reapox, D523) at relative humidities 33, 53, 75, 84, and 97% at a temperature of 50 °C. The experimental data were modeled using both Fickian and Langmuir. Figure 2.16 displays the moisture content versus square root of time ($h^{1/2}$) for the epoxy specimens at relative humidities (RH) and predictions based on Fickian and Langmuir models.

They found a good fit to the 33% RH data by the Fickian model, Fig. 2.16a. At higher humidities the Fickian model did not fit the data at intermediate times, The Langmuir model, Fig. 2.16b, however, provides a good fit to the data over the entire range of RH.

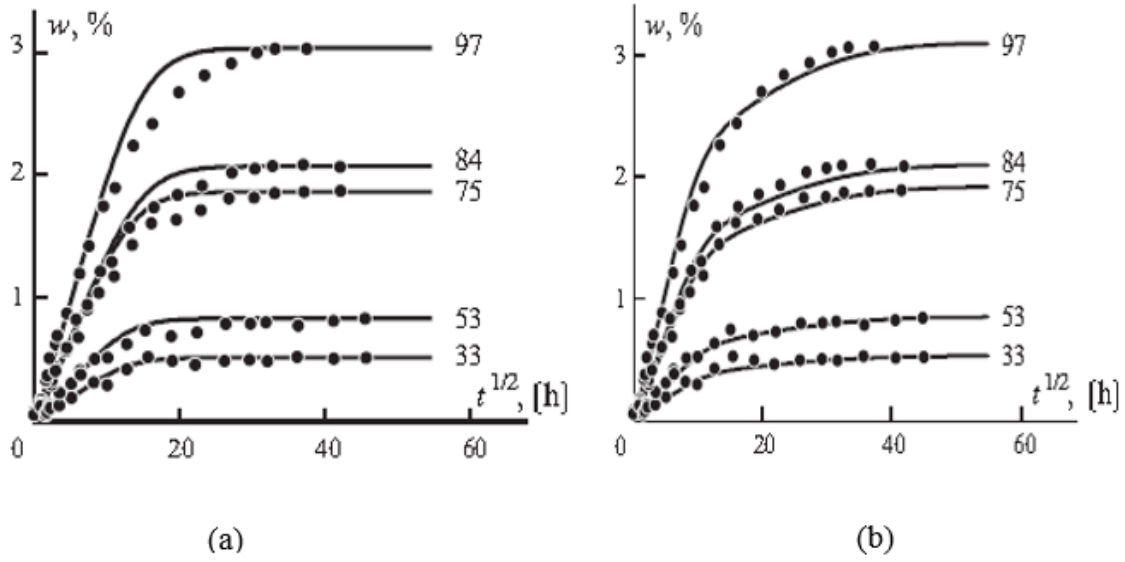

Figure 2.16 Moisture content vs. square root of time (h) for epoxy specimen at different relative humidities, Experimental data are shown as points, model results are shown as solid curves (a) Fickian model, (b) Langmuir model, Glaskova et al. (2007).

2.5.2 Micromechanics Models

The analogy between the moisture diffusivity and electrical conductivity can be used to analyze the moisture diffusivity in the void containing specimens. The diffusivity of the void containing specimens may be determined using micromechanical analysis.

Micromechanical analysis is the analysis of heterogeneous composite materials based on the individual constituents or phases in these materials.

Maxwell (1873) derived a model for predicting the electrical conductivity of a material with spherical particles distributed in a homogeneous matrix, see Pal (2007). Using the analogy between Maxwell model, the moisture diffusivity for the void containing specimens can be expressed as follows,

$$\frac{D}{D_r} = 1 + 3\left(\frac{D_a - D_r}{D_a + 2D_r}\right)v_v \tag{2.23}$$

where D_r is resin moisture diffusivity, D_a is the air diffusivity, v_v is the volume fraction of the voids.

As the resin moisture diffusivity D_r is much smaller compared to the air diffusivity D_a, Eq. (2.23) can be simplified,

$$\frac{D}{D_r} = 1 + 3v_v \tag{2.24}$$

Eq. (2.24) predicts the diffusivity of the void containing specimens being a linear function of the void content.

3 EXPERIMENTAL

Epoxy resin is selected for the study of water uptake in void-free and void containing polymers. Epoxy absorbs moderate amounts of water and void-free epoxies have beenexamined in many previous studies, e.g. Adamson(1980), Perrin et al. (2009).

Specimens without and with voids were prepared. Void shape, size and content were determined using optical microscope, image analysis, and density measurements. DSC and DMA tests were conducted on dry specimens to verify that the foaming chemicals did not influence the chemistry of the host polymer. Water uptake by void-free and void containing epoxy specimens was monitored by weighing specimens immersed in distilled water at 40 °C. The state of water in the moisture-aged void-free and void containing specimens was analyzed by DSC analysis. The moisture swelling strain was measured to further examine how sorbed water influenced the swelling of the polymer.

3.1 Materials

Epoxy plastics are formed by mixing epoxy resin with a curing agent. The curing agent is a chemical that reacts with the resin to achieve a polymer with cross-linked chains. This process is called “cure”. The epoxy resin (Epon^{TM} 828) is manufactured by Hexion Company (US). The chemical name of Epon 828 is Bisphenol-A diglycidyl ether epoxy and the chemical structure is described in Fig. 3.1

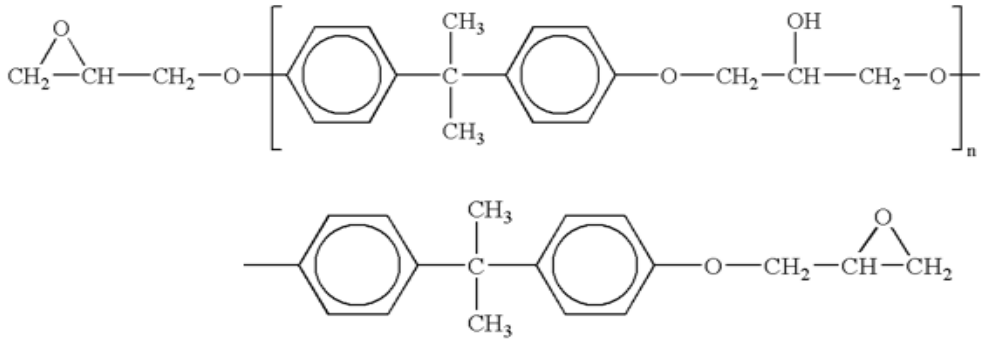

Figure 3.1 Chemical structure of Epon 828 epoxy. n is changed from 0 (fluids) to 25 (hard solids).

Amine curing agent (Epikure™ 3072) manufactured by Hexion Company (US) is utilized. The main components are polyethylene polyamine (70-90%), diethylenetriamine (7-10%), and tetraethylenetriamine (7-10%). The amine chemical structure is shown in Fig. 3.2.

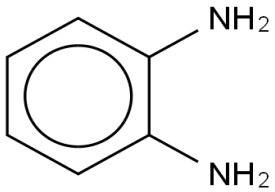

Figure 3.2 Chemical structure of amine curing agent.

During cure, the reactive side groups in the amine curing agent form cross links with the epoxide groups at the ends of the epoxy molecule, Fig. 3.1, and form a tight covalently bonded network.

To create voids, foaming agents were used. Foaming agents generates hydrogen gas during the curing process of the epoxy/amine which creates cavities (voids) inside the material. Ploymethylhydrosiloxane (PMHS), manufactured by Sigma Aldrich Company, which is stable to air and moisture, and nontoxic was used as one of the foaming agents. The chemical structure of PMHS is shown in Fig. 3.3a. The other foaming agent,

fluoro/dimethylsiloxane copolymer (POMSC) “surfactant” was obtained from Momentive Company. The chemical structure is shown in Fig. 3.3b.

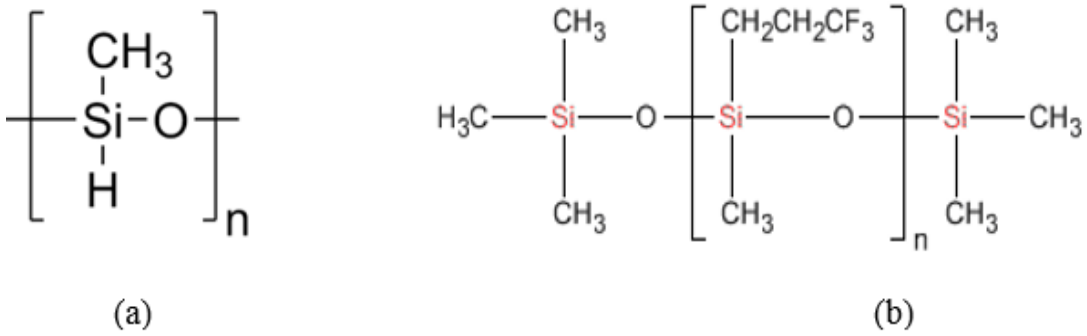

Figure 3.3 Chemical structure of foaming agents. a) PMHS, b) POMSC.

Mixing ratio refers to the ratio of mass of added substance (amine, PMHS, POMSC) to mass of epoxy resin. The mixing ratios of the void containing epoxy specimens were guided by a previous study on epoxy foams, Wang (2013). The mixing ratios are listed in Table 3.1. Mixture (a) did not include POMSC, while mixture (b) included POMSC at a ratio of 0.01. Void-free epoxy specimens were prepared using two amine ratios (0.3 and 0.35). For the low void content specimens, amine was first added to the epoxy at a ratio of 0.3 after which POMSC was added. Finally, amine was added at a ratio of 0.05. For the medium void content specimens, PMHS was added. High void content specimens were prepared using two recipes. When adding any chemical ingredient to epoxy, the mixture was stirred for 3 min.

Table 3.1 Composition (mixing ratios) of void-free and void containing specimens (Epoxy=1.0).

Specimen	Amine	PMHS	POMSC
Void free (a)	0.3	0	0
Void free (b)	0.35	0	0
Low void content	0.35	0	0.01
Medium void content	0.35	0.003-0.004	0
High void content (a)	0.35	0.01	0
High void content (b)	0.35	0.01	0.01

3.2 Water Absorption Test Specimens

Test specimens in the form of a circular plate of 50.8 mm diameter and 5.08 mm thickness (Fig. 3.4a) were prepared by casting uncured resin (Table 3.1) in an open circular mold cavity, Fig. 3.4b. 5-7 replicate specimens were made. The resin samples were cured for at least 14 days at room temperature (25 °C) according to specifications from the epoxy resin manufacturer.

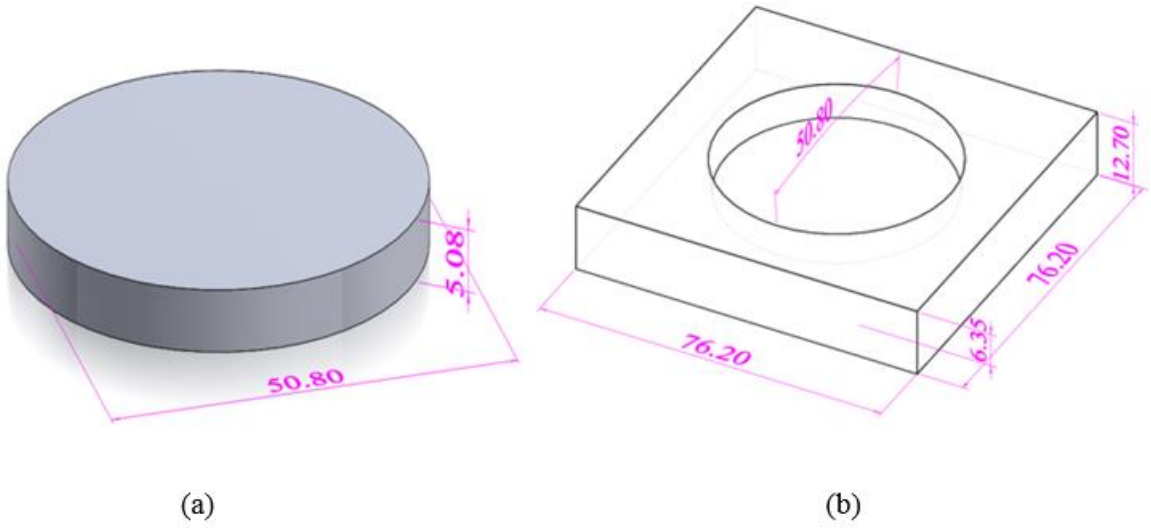

Figure 3.4 Epoxy sample a) specimen dimensions, b) Open polyethylene mold. All dimensions are in mm.

3.3 Microstructural Characterization

Cross sections of epoxy specimens (void free, low, medium and high void content) were examined in an optical microscope (Versamet-2 Unitron-7011) to analyze the void geometry and determine void size and void content, Little et al. (2012), Paciornik and d'Almeida (1999). Specimens were first sectioned with a circular blade saw. To obtain a sample holder, the specimen were cast in epoxy in a 3.81 cm diameter mounting cup (Buehler Company). The cut cross section was sanded using 240, 320, 400, and 600 grit papers. The final step was polishing using a micro-cloth coated polishing wheel using water solutions with 5 and 1 micron aluminum-oxide particles. A flat surface with a mirror-like finish was achieved after the polishing process.

ImageJ software, Rasband (1997) was utilized to determine the void size and void content. This software extracts the image information from a digital image using the image processing technique as explained earlier in Section 2.3.2. The voids are detected by ImageJ as they are generally darker than the epoxy resin. Void area fraction is used to estimate the void volume fraction. Kuo and Frost (1996), Hilliard (1968) and Papthanasiou and Guell (1997) show that the area-to-volume conversion is justified if the voids are close to spherical in shape and distributed randomly inside the specimen. The image analysis requires calibrating the size of the image by viewing a small ruler. Hence, images that include a measuring scale were used to achieve calibrated length units (e.g. mm).

Figure 3.5 shows an example of a cross section of a sample containing voids with a mm scale included. The steps of ImageJ analysis are outlined in Fig. 3.5. First, the original image (Fig. 3.5a) is converted to a binary image (8 bite), Fig. 3.5b. Then, the gray scale image is changed to a black and white image by adjusting the image threshold. The voids

are clearly distinguished as black dots in the image, see Fig. 3.5c. The number of voids is counted and their area are measured. The void content is estimated from the total area of voids divided by the image area. Void size is expressed as an effective diameter determined from the void area.

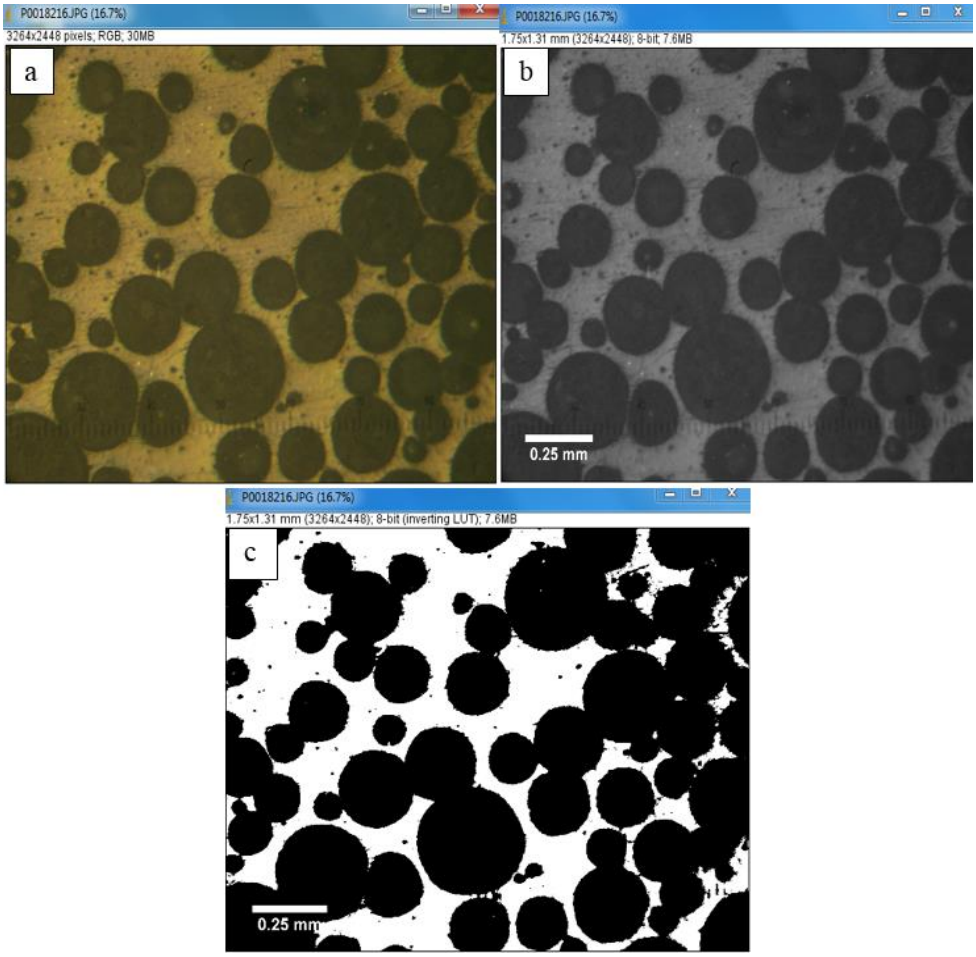

Figure 3.5 Micrographs of cross section of high void content panel (v_v=56.0%). a) original image JPG, b) image after the scale is settled and converted to 8 bite, and c) image after the threshold is adjusted and the image is converted to black and white.

3.4 Differential Scanning Calorimetry (DSC)

For our study, a major concern is whether or not the foaming agents added to the polymer changes the basic chemistry of the epoxy resin. A change in T_g would indicate changes of

the chemistry of the polymer. DSC analysis was therefore conducted on dry void-free and void containing epoxy specimens. The DSC analysis method is described in Section 2.4. DSC testing was performed on dry void-free and void containing epoxy specimens with a TA instrument DSC model Q10-V9.0 Build275. The DSC tests were run using a heating/cooling cycle where the specimen is heated from room temperature (RT) to 250 °C, then cooled to RT. Both heating and cooling rates were set at 10 °C/min.

For each DSC test, a small amount of material (5-10 mg) is extracted from a specimen and placed in a DSC aluminum pan after which the lid is closed using a press. In addition, an empty (reference) pan covered with a lid was used. The sample and the reference pans were placed inside the DSC cell. The DSC tests were run under a constant flow of nitrogen (50 ml/min) to prevent oxidation of the test specimen.

3.5 Dynamic Mechanical Analysis (DMA)

The DMA test principle is described in Section 2.5. DMA tests were run on void-free and void containing epoxy specimens on a TA instruments DMA Q800. The purpose of the DMA tests was to further verify the consistency of chemistry of the void containing specimens, in addition to the DSC tests.

Rectangular dry epoxy beam specimens of dimensions 36 × 9.30 × 3.2 (mm) were loaded in a three-point bending fixture at an amplitude of 15 μm and frequency of 1 Hz. The temperature range was from 30 to 200 °C at a heating rate of 5 °C/min. The components (E' and E'') of the complex modulus (E*) were determined as a function of temperature. The glass transition temperature T_g is estimated from the location of the peak in the loss modulus (E'') vs. temperature curve.

3.6 Water Up-take Specimens

3.6.1 Specimen Conditioning

Specimens for the water immersion test in the form of circular plates, Fig. 3.4a, were sanded and polished. Then, specimens were dried for 24 h in a furnace (model 20 GC lab oven) at 51 °C according on ASTM D5229 (1998). After drying, the specimens were kept in a desiccator. The test program for the water uptake experiment is provided in Table 3.2. Specific void-free and different void contents containing specimens were selected for water aging program based on the consistency of epoxy resin chemistry, which will be discussed later.

Table 3.2 Test specimens for water absorption.

Specimens	Void content (v_v) %
Void free (a)	**0.32, 0.13**
Medium void content	**26.6, 26.7, 27.6**
High void content (a)	**39.8, 54.1, 59.1**

3.6.2 Water Aging Program

The water aging program was initiated by weighing dry specimens in a Sartorius analytic balance accurate within ±0.1 mg. To allow immersion of the void containing specimens (with density less than water), a sample holder was designed and built from high density polyethylene to hold up to eight specimens, see Fig. 3.6. Acrylic plastic rods were snap fitted on top of each specimen to prevent specimens from floating. The sample holder and specimens were immersed in distilled water at 40±1 °C in a temperature controlled tank at (PolyScience 2H1341878). To monitor water uptake, specimens were periodically withdrawn from the water bath one by one, and wiped dry using a paper cloth and weigh in the Sartorius analytic balance. The moisture content is calculated from the weight gain:

$$\mathbf{M(t)} = \frac{\mathbf{m(t)-m_0}}{\mathbf{m_0}} \tag{3.1}$$

where m(t) is the mass of the specimen after absorbing moisture for a specified time (t) and m_0 is the mass of the dry specimen.

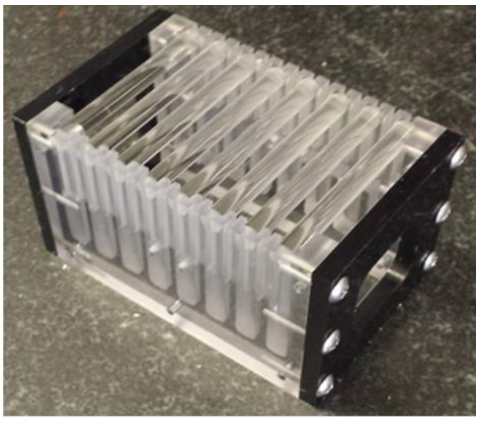

Figure 3.6 Photo of moisture aging sample holder.

3.6.3 Swelling

Moisture swelling strain is defined as the relative volume increase upon water saturation, Adamson (1980), and González et al. (2012),

$$\frac{\Delta V}{V_0} = \frac{V_\infty - V_0}{V_0} \tag{3.2}$$

where V_0 and V_∞ are the volumes of the dry and saturated specimen.

After 417 days of immersion, the circular disk specimens were withdrawn from the water tank and wiped off using paper cloth. A caliper accurate within ±0.02 mm was used to measure the diameter (D) of the specimen and the thickness (h) was measured with a micrometer accurate within ±0.005 mm. The swelling strain was determined from Eq. (3.2) based on the calculated volumes of the saturated and dry specimens ($V = \pi D^2 h/4$).

3.6.4 DSC Test for Moisture Aged Specimens

DSC analysis of water-aged epoxy specimens was used to examine the state of water as discussed in Section 2.6.3. All tests were performed in a TA instrument model Q10-V9.0 Build275. To allow testing at low temperatures, the test cell was connected to a cooling unit.

Small DSC samples (7-15 mg) were cut from larger dry samples using diamond cutter. A plastic clip and string were used to suspend and immerse the dry small DSC samples in a distilled water tank at 40 °C. The samples were kept in the distilled water tank for 7-15 days to absorb water. Prior to DSC testing, the surface of the samples was wiped dry by a paper cloth.

For each test, a DSC sample and a reference (an empty aluminum pan covered with a lid) were placed inside the DSC unit and were exposed to a cooling cycle from room temperature (RT) to -80 °C at a rate of 10 °C/min. After cooling, the specimens were heated to RT. The DSC measurements were run on specimens with the full range of void contents.

As discussed in section 2.6.3, the sorbed water may be categorized into free water, freezable bound water and non-freezable bound water. The temperatures and enthalphies for the transitions were recorded in the cooling and heating cycles, see Fig. 2.11 (Section 2.6.3). The enthalphy of each transition was determined from the area under the peak to allow calculation the contents of free and bound water. The DSC test matrix is provided in Table 3.3, which lists the number of specimens, void content, and time of immersion.

Table 3.3 DSC Test Matrix for water-aged specimens. "F", "M" and "H" represents void-free, medium and high void content.

Void Content %	Designation	Number of tests	Immersion time (days)/ # specimens
0	**SPF-3**	**1**	**0**
2.47	**SPF-2**	**2**	**7/1, 15 /1**
26.6	**SPM-7**	**2**	**7/1, 15/1**
41.7	**SPH-6a**	**2**	**7/2, 15/1**
55.9	**SPH-7a**	**1**	**15/1**

Table 3.4 summarizes the overall test program where the numbers indicate the number of replicate specimens.

Table 3.4 Overall test program. Numbers represent the number of replicate test specimens.

Specimen	Microstructure	Density	DSC (dry)	DMA (dry)	Moisture uptake	Moisture swelling	DSC (wet)
Void free (a)	1	6	2	1	2	2	2
Void free (b)	1	4	2	--	--	--	--
Low void content	1	6	2	--	--	--	--
Medium void content	1	5	2	1	3	3	1
High void content (a)	1	6	2	1	3	3	2
High void content (b)	1	7	2	--	--	--	--

4 EXPERIMENTAL RESULTS

4.1 Density (Archimedes method)

Density was measured to determine the void content as explained in section 2.3.3. The density of specimen (ρ) is defined as mass of the specimen (m) divided by its volume (V). The specimen volume may be calculated from the specimen dimensions using e.g. digital caliper and micrometer. Another method to determine the volume is to use Archimedes method, Hughes (2005). This method utilizes air and hydrostatic weighing (underwater weighing) to measure the volume. The Archimedes principle states the volume of a specimen immersed in water (cm^3) is equal to the weight of water (g) that it displaces. This method, obviously does not work well for materials with density less than water (ρ_w=1 g/cm^3) since they will float on the surface of water. Only the void-free samples have density higher than 1 g/cm^3.

The density of void-free epoxy specimens was determined by both Archimedes method and from weight and dimensional measurements. Using an analytical balance accurate within ±0.01mg, the specimen was first weighed in air (m_1). A beaker containing distilled water at 19 ºC and a wire (used to suspend the specimen) was placed on the balance and the weight (m_2) of the water and beaker was determined. Then, the specimen was suspended in the water above the bottom of the beaker using a wire and stand arrangement. The specimen weight is now partly supported by the wire and partly by the buoyancy of the displaced water. The weight (m_3) was recorded. The mass of displaced water, according

to Archimedes principle, is $m_4 = m_3 - m_2$ (g). The volume of specimen is given by $V = \frac{m_4}{\rho_w}$ where ρ_w is the density of water (1 g/cm^3). The density of the specimen is given by,

$$\rho = \frac{m_1}{V} \tag{4.1}$$

A direct method to determine the specimen density is to calculate the volume based on measured specimen dimensions (diameter and thickness). We used a digital caliper and a micrometer accurate within ±0.02 and ±0.005 mm. Results from the density measurements of the void-free specimens are provided in Table 4.1. Both methods provide similar results. The average density, 1.153 g/cm^3 is close to the density of epoxy provided by the resin manufacturer (Technical data sheet, Hexion) $\rho = 1.16$ g/cm^3. Density of the void containing specimens was determined from measured weight and specimen dimensions.

Table 4.1Density of void-free epoxy specimens determined by Archimedes method and specimen dimensions, where m_1 (mass in air), m_4 (mass of displaced water), V (volume), ρ (specimen density), and ρ_w (water density =1 g/cm^3).

Specimen #	m_1 (g)	m_4 (g)	ρ (g/cm^3) Archimedes	ρ (g/cm^3) measured dimensions
SP-1	10.79	9.29	1.16	1.17
SP-2	10.17	8.81	1.16	1.13
SP-6	11.18	9.62	1.17	1.15
S-1	11.09	9.68	1.15	1.14
S-2	10.74	9.38	1.15	1.14

4.2 Microstructural Analysis

Figure 4.1 shows examples of micrographs of polished cross sections cut from void-free, low, medium, and high void content specimens. The micrographs show voids as dark inclusions. The shape of voids is close to circular, which for 3D, would correspond to spherical voids. The micrograph in Fig. 4.1a shows a cross section of a void-free specimen although small isolated voids are observed. The image of the low void content specimen in

Fig. 4.1b shows isolated voids and large number of small barely visible voids distributed uniformly. The micrograph for the medium void content specimen, Fig. 4.1c, displays some large voids and several smaller voids. Most of the larger voids are isolated by a thick wall. The high void content specimen, Fig. 4.1d, displays many large voids. Although several of the large voids are separated by a thin wall, many voids merge forming connected voids, see Fig. 4.1d.

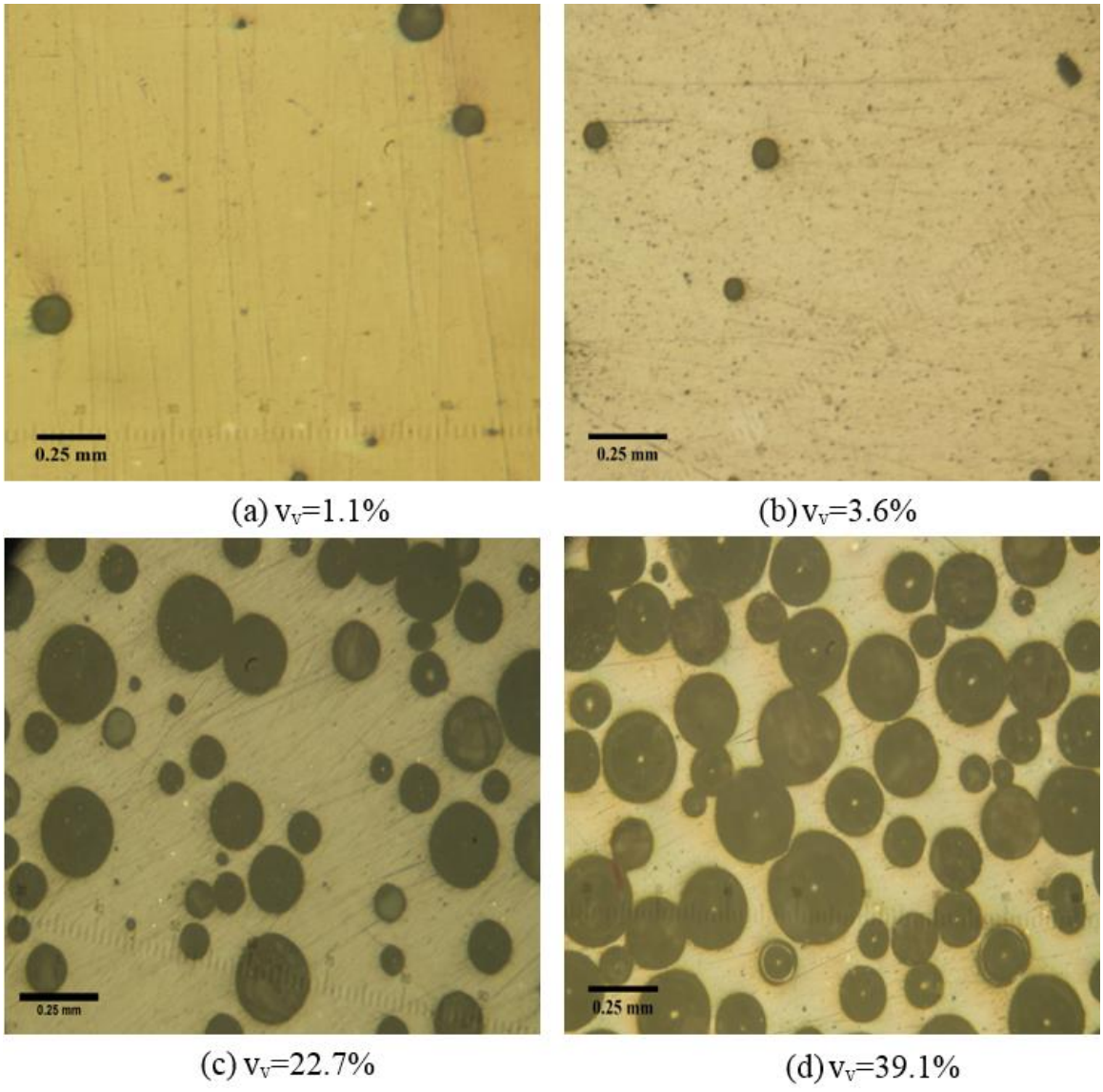

Figure 4.1 Micrographs of void-free and void containing specimens. a) void-free (SP-3), b) low void content (SPL-2), c) medium void content (SPM-1), and d) high void content a (SPH-2a).

4.3 Void Content

Void contents determined from the density based on measured weight and dimensions are summarized in Tables 4.2 - 4.6.

Table 4.2 Density and void content for void-free specimens (a), reference density ρ =1.16 g/cm^3.

Specimen #	Density g/cm^3	Void Content %
SP-1	**1.17**	**-0.58**
SP-2	**1.13**	**2.47**
SP-3	**1.17**	**-0.64**
SP-4	**1.16**	**0.315**
SP-5	**1.16**	**0.132**
SP-6	**1.15**	**1.14**
		$v_v = 0.47 \pm 1.18$

Table 4.3 Density and void content for low void content specimens.

Specimen #	Density g/cm^3	Void Content %
SPL-1	**1.06**	**8.72**
SPL-2	**1.11**	**4.26**
SPL-3	**1.15**	**1.28**
SPL-4	**1.14**	**1.61**
SPL-5	**1.14**	**2.20**
SPL-6	**1.13**	**2.28**
		$v_v = 3.4 \pm 2.8$

Table 4.4 Density and void content for medium void content specimens.

Specimen #	Density g/cm^3	Void Content %
SPM-1	**0.85**	**26.9**
SPM-2	**0.84**	**27.6**
SPM-3	**0.82**	**29.7**
SPM-4	**0.85**	**26.7**
SPM-5	**0.85**	**26.7**
SPM-6	**0.81**	**30.6**
		$v_v = 28.0 \pm 1.7$

Table 4.5 Density and void content for high void content specimens (a).

Specimen #	Density g/cm^3	Void content %
SPH-1a	**0.70**	**39.9**
SPH-2a	**0.64**	**44.7**
SPH-3a	**0.53**	**54.1**
SPH-4a	**0.48**	**59.1**
SPH-5a	**0.46**	**60.4**
		$v_v = 51.6 \pm 9$

Table 4.6 Density and void content for high void content specimens (b)

Specimen #	Density g/cm^3	Void content %
SPH-1b	**0.53**	**54.1**
SPH-2b	**0.62**	**46.1**
SPH-3b	**0.62**	**46.6**
SPH-4b	**0.58**	**50.3**
SPH-5b	**0.54**	**53.6**
SPH-6b	**0.58**	**49.8**
SPH-7b	**0.54**	**53.5**
		$v_v = 50.6 \pm 3.3$

Void contents of the void-free specimens range between -0.64 to 1.14%, Table 4.2. Negative void content is of course impossible but may be a result of density variations or error in the density measurements. The average void contents for the void-free, low void, medium void, high void (a), and high void (b) content specimens are 0.47, 3.4, 28, 51.6, 50.6 % respectively. The void contents do not show much variability, except for one low void content specimen SPL-1, Table 4.3, and the high void content specimens (a) SPH, Table 4.5. The small variability indicates consistent specimen preparation.

The void contents determined from ImageJ analysis and density method are shown in a bar chart in Fig. 4.2. The void content results determined by the two methods are close.

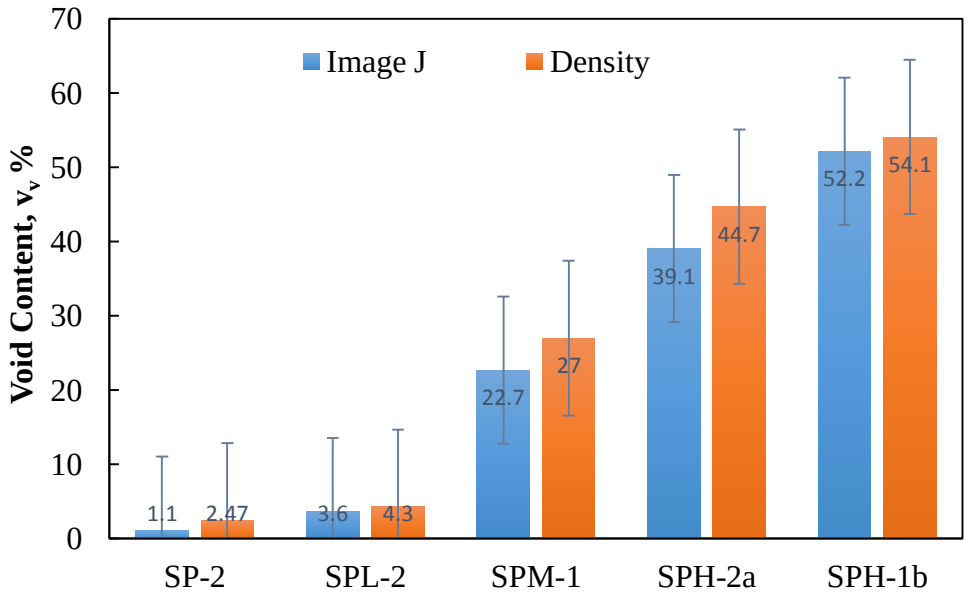

Figure 4.2 Void content from Image analysis and density measurements.

Image analysis was conducted on the micrographs to quantify void dimensions and void content as explained earlier. Figure 4.2 shows examples of void size distributions in medium and high void content specimens for voids with diameter greater than 50 µm. The void size distributions indicate voids with diameters in the range from 50 to 350 µm, with averages of 120 and 150 µm for the medium and high void content specimens. The largest voids are significantly smaller than the thickness (5.08 mm) of the moisture aging specimens.

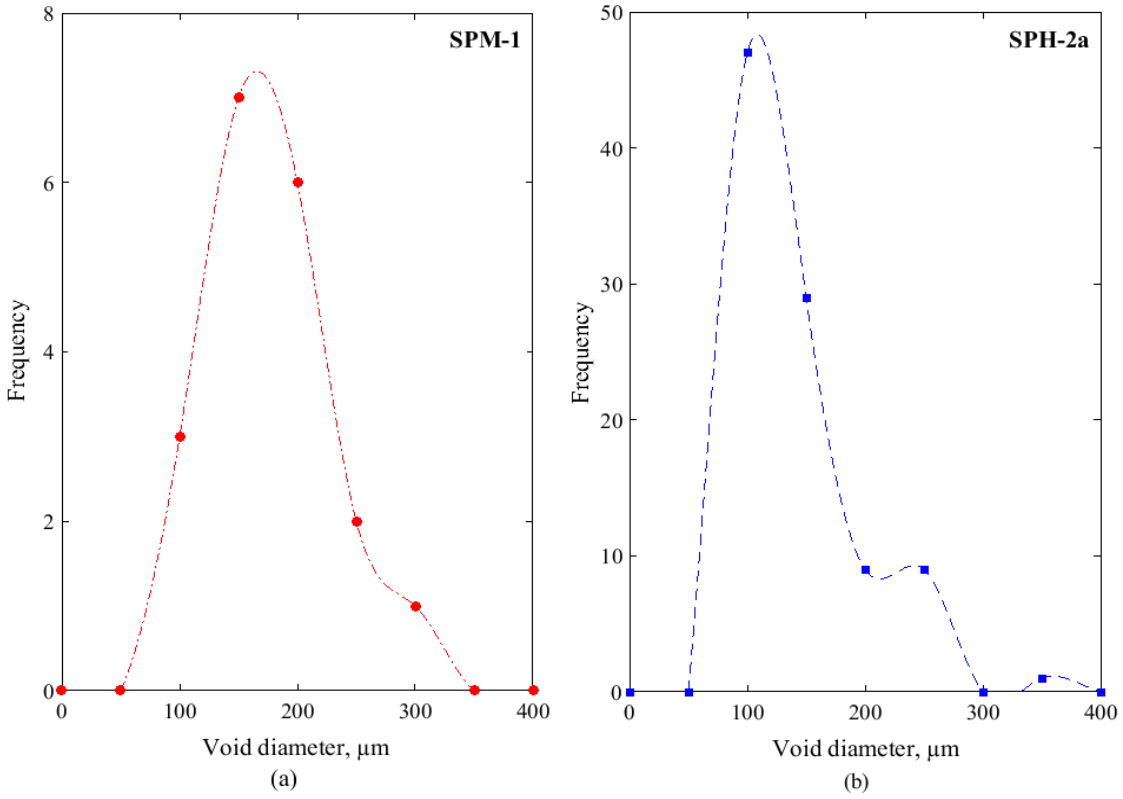

Figure 4.3 Void size distributions. a) medium void content SPM-1, v_v= 26.9%, b) high void content SPH-2a, v_v= 44.7%.

4.4 DSC Results for Dry Specimens

DSC analysis was performed on void-free and void containing dry specimens, specifically SP-6 v_v=1%, SPL-3 v_v=4%, SPM-1 v_v=27%, SPH-5a v_v= 60%, and SPH-4b v_v=51% to determine the glass transition temperature (T_g). DSC was conducted on two replicate specimens after drying inside a furnace at 51 °C for 24 h.

Examples of DSC curves for void-free and medium void content specimens are shown in Fig. 4.4. Glass transition temperatures, T_g, for these specimens are close, 90.2 and 90.1 ºC. Glass transition temperatures for the all specimens are summarized in Table 4.7.

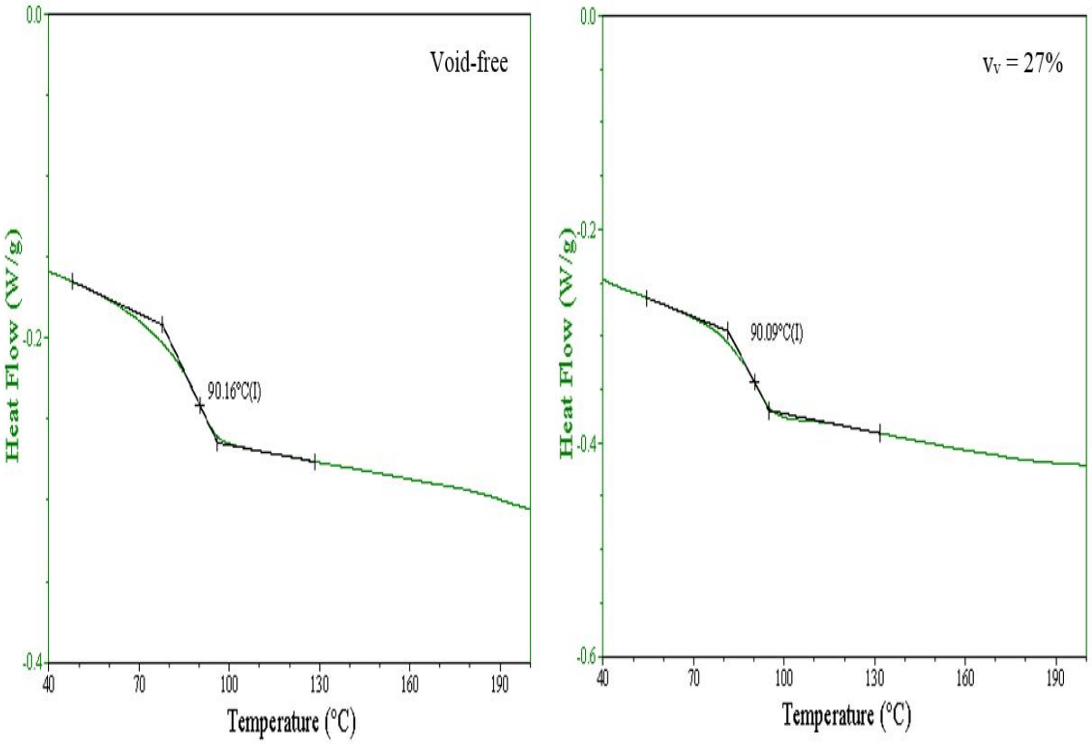

Figure 4.4 DSC curves for dry epoxy specimens. a) void-free specimen, b) medium void content (SPM-1, v_v= 27 %).

Table 4.7 Glass transition temperature determined from DSC tests.

Epoxy Specimens	v_v%	T_g, °C	
		1st Test	2nd Test
Void-Free 1st	1	90.3	89.0
Void-Free 2nd	2	89.4	--
Low void content	4	81.1	80.9
Medium void content	27	90.4	93.3
High void content (a)	60	92.9	92.1
High void content (b)	50	89.1	95.0

T_g values are close to 90 °C for all specimens except for both replicates of the low void content specimen with a T_g of about 81 °C. Zhou and Lucas (1999) reported T_g = 90 °C for Epon 828. The low T_g of the low void content specimens indicates that the cross link structure is affected by adding the POMSC foaming agent (Table 3.1). Also, the micrograph of the low void content specimen shown in Fig. 4.1b indicates a porous

structure with a large number of very small distributed voids, different from the other epoxy specimens with larger discrete voids.

The specimens used in the water aging program were selected based on their T_g values which should be close to the void-free epoxy specimen (about 90 ºC). Hence, the low void content specimens (SPL) and the high void content specimens (SPH-b) were excluded from further study.

4.5 DMA Results for Dry Specimens

DMA testing provided the storage and loss moduli, and tan δ for void free, medium void content, and high void content epoxy specimens. Figure 4.5 shows the storage and loss moduli plotted vs. temperature. The storage modulus (E') of the void-free and medium void content specimens in the glassy region is in the GPa range. For the specimen with a high void content, the modulus E' is below the GPa range. The glass transition leads to large drops in storage and loss moduli.

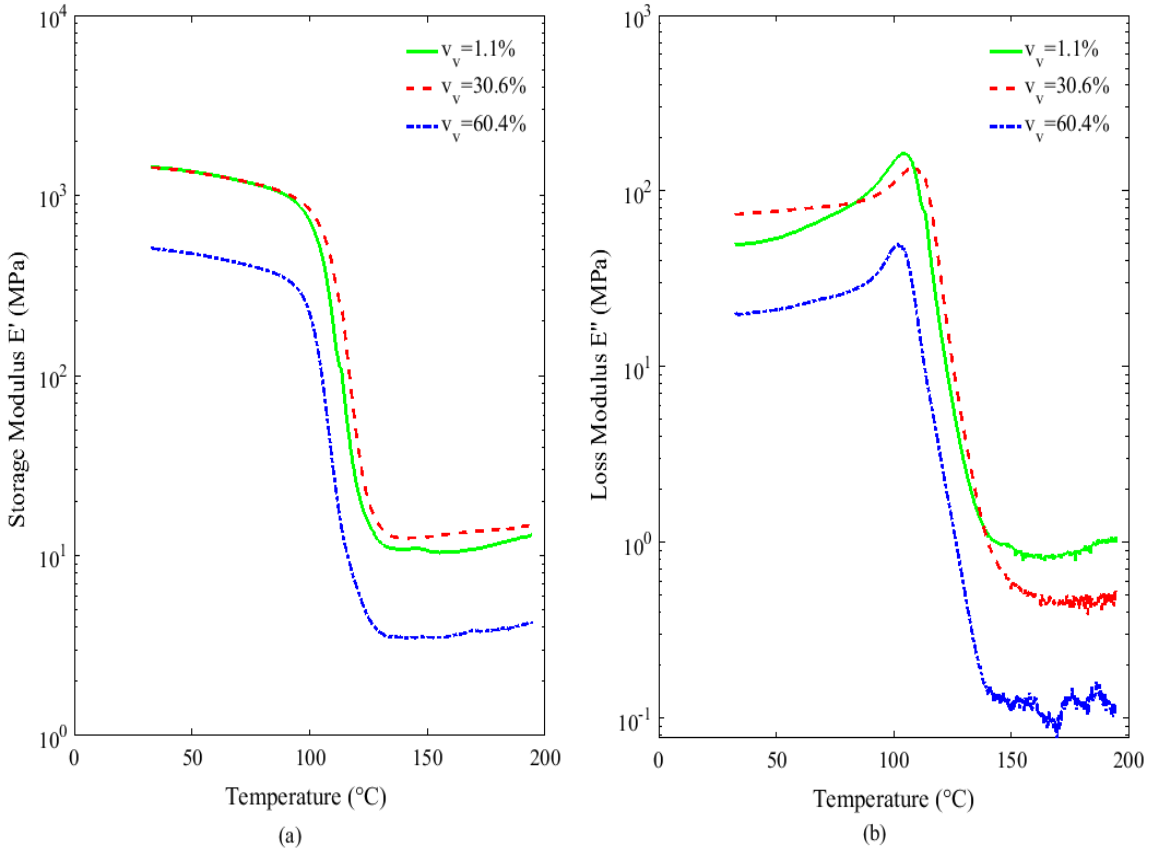

Figure 4.5 Storage (a) and loss (b) moduli vs. temperature for void free (v_v = 1.1%), medium (v_v = 30.6%) and high void content (v_v = 60.4%) epoxy specimens.

Figure 4.6 shows the loss tangent plotted vs. temperature for void-free, medium and high void content specimens. At the transition, the peak temperatures are close.

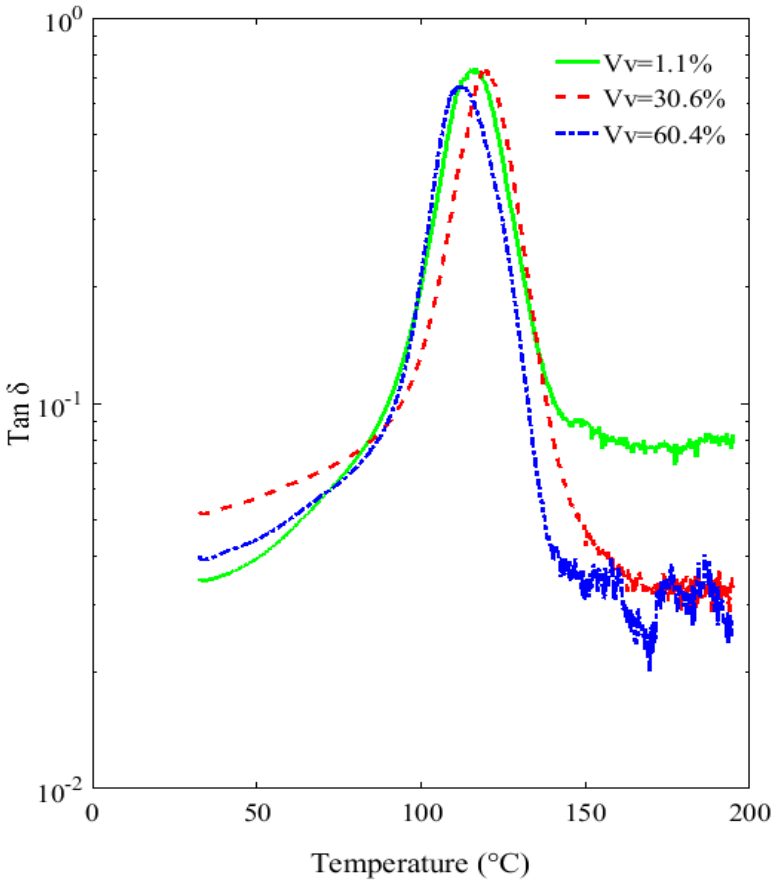

Figure 4.6 tan δ. vs. temperature for void free (v_v = 1.1%), medium (v_v = 30.6%) and high void content (v_v = 60.4%) epoxy specimens.

The peak of the loss modulus is a common measure of the glass transition temperature T_g, Aklonis and MacKnight (1983). T_g values are summarized in Table 4.8. The T_g values are consistent and varies in a narrow range from 102-109 ºC. The void-free, medium void and high void content epoxy specimens have similar T_g values, which indicates consistency of chemistry in the void-free and void containing specimens.

The T_g results from the DMA test (Table 4.8) differ from those obtained from the DSC test, where T_g values of about 90 ºC are observed. Aklonis and MacKnight (1983) pointed out that DSC and DMA tests produce different T_g values because of the different time scales and principles of the tests.

Table 4.8 Glass transition temperatures determined by DMA.

Specimen	v_v %	T_g (°C)
SP-1	1.1	105
SPM-6	30.6	109
SPH-5a	60.4	102

4.6 Water Up-take

The weight gain of the wet test specimens was periodically measured. Moisture content was monitored during 403 days of immersion (as of Mar. 2018). Figure 4.7 shows moisture content vs. square root of time ($\sqrt{\text{day}}$) plots for the void-free, medium and high void content specimens.

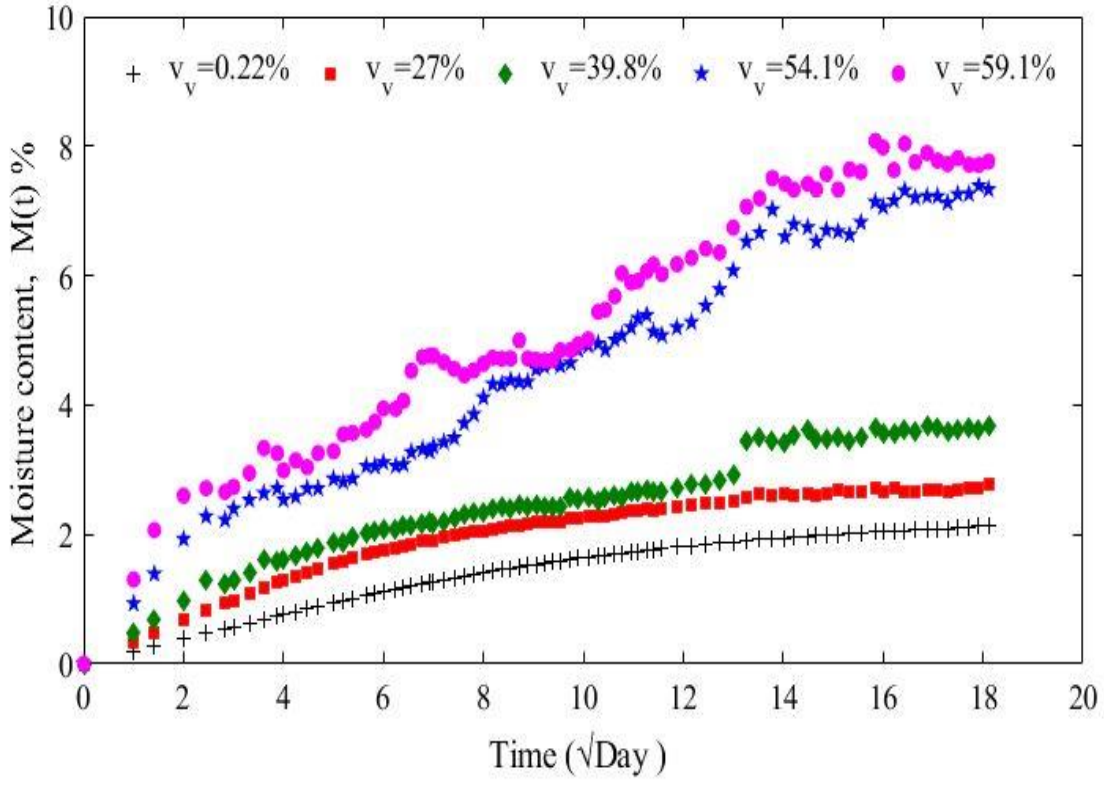

Figure 4.7 Moisture content vs. square root of time (√Day) for void-free, medium, and high void content epoxy specimens.

The water uptake occurs faster and reaches higher moisture contents when the void content increases, see Fig. 4.7. The moisture contents for the high void content specimens show oscillations. The reason for such behavior is not known, but may possibly be due initially slow water penetration through the relatively small "walls" between voids (Fig. 4.1d), followed by more rapid entry of water molecules into the empty void cavity. All specimens are essentially saturated. The maximum moisture content reached by the various specimens after 403 days of immersion is shown in Fig. 4.8. The moisture uptake is obviously amplified by the presence of voids.

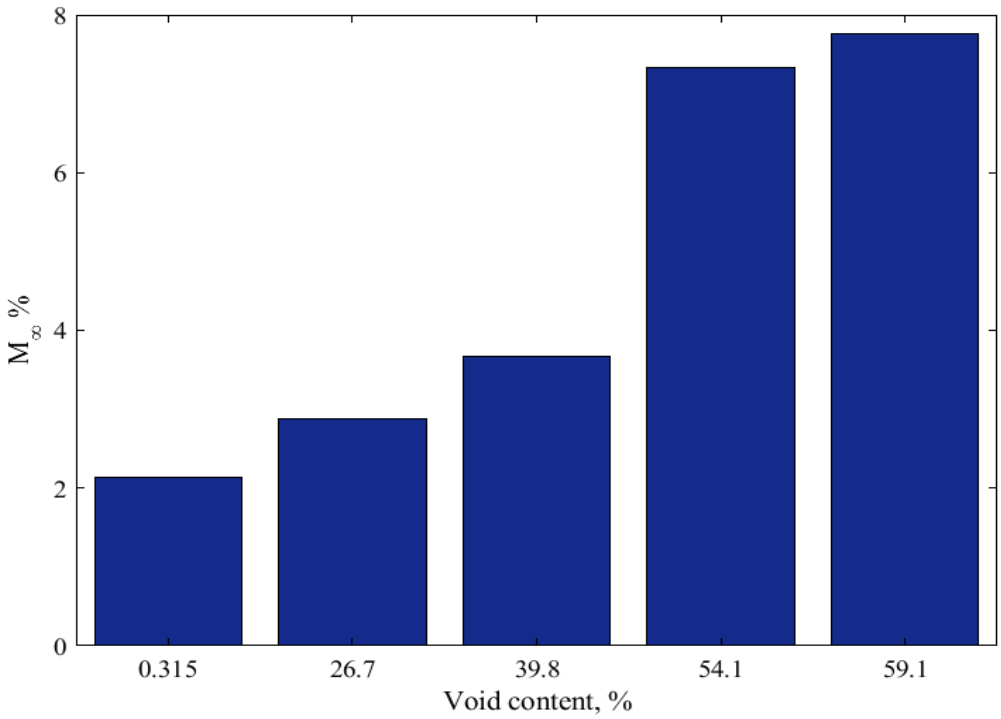

Figure 4.8 Moisture content after 403 days of immersion vs. void content.

5 MOISTURE UP-TAKE ANALYSIS

5.1 Fickian Model

As discussed in Chapter 2 the water uptake process in polymeric materials is commonly assumed to follow Fick's law. For 1D diffusion, the moisture content M(t) is given by,

$$M(t) = \begin{cases} M_\infty \frac{4}{h}\sqrt{D}\sqrt{\frac{t}{\pi}} \quad , & \frac{Dt}{h^2} < 0.05 \qquad (5.1a) \\ M_\infty \left[1 - \frac{8}{\pi^2} e^{\left(-\frac{Dt}{h^2}\pi^2\right)}\right] \quad , & \frac{Dt}{h^2} > 0.05 \qquad (5.1b) \end{cases}$$

where M_∞ is the saturated moisture content, D is the diffusivity (m^2/s), h is the polymer panel thickness (m), and t is the time (s).

Fick's law was first applied to the void-free specimen. The diffusivity, D, was determined from initial linear slope of the M(t) vs. $\sqrt{t}$ data and saturation moisture content, M_∞, estimated from the experimental trend, Fig. 4.7, and Eq. (5.1a) as explained in Chapter 2. Figure 5.1 displays Fickian model and experimental data for the void-free specimen.

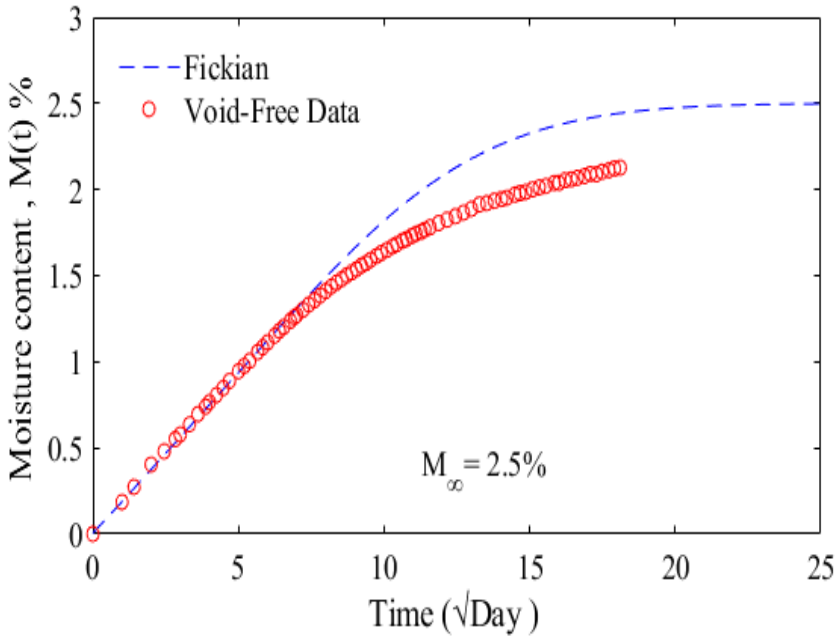

Figure 5.1 Fickian model predictions and experimental data for void-free specimen.

The Fickian model results shown in Fig. 5.1 fits the data at shorter times ($\sqrt{t}$ < 8 days$^{1/2}$). For longer immersion times, the Fickian model overpredicts the moisture uptake.

5.2 Langmuir Model Analysis of Experimental Data

The Langmuir model is described in Section 2.7.1. The moisture content predicted by the 1D Langmuir model is expresssed as follows, Bonniau and Bunsell (1981),

$$M(t) = \begin{cases} M_\infty \cdot \frac{\alpha}{\alpha+\beta} \cdot \frac{4}{\pi} \cdot \sqrt{\frac{Dt}{h^2}} \quad , \quad \frac{Dt}{h^2} < 0.05 & (5.2a) \\ M_\infty \left[1 - \frac{\beta}{\alpha+\beta} exp(-\alpha t) - \frac{\alpha}{\alpha+\beta} \cdot \frac{8}{\pi^2} exp\left(-\frac{\pi^2 Dt}{h^2}\right)\right] \ , \ \frac{Dt}{h^2} > 0.05 & (5.2b) \end{cases}$$

Bonniau and Bunsell (1981) proposed,

$$\alpha = \frac{D}{h^2}, \qquad \beta = \frac{3\alpha}{7} \qquad (5.3a, b)$$

The diffusivity D was evaluted for all specimens from the short-time experimental data moisture uptake data using Eq. (5.2a). The saturated moisture content M_∞ was estimated

from the asymptotic trend shown in Fig. 4.7. The parameter β was estimated as $\beta = \frac{2\alpha}{3}$ which provides better fit than Eq. (5.3b) to our data.

Figure 5.2 shows experimental moisture content for the void-free, medium and high void content specimens and prediction from Eqs. (5.2).

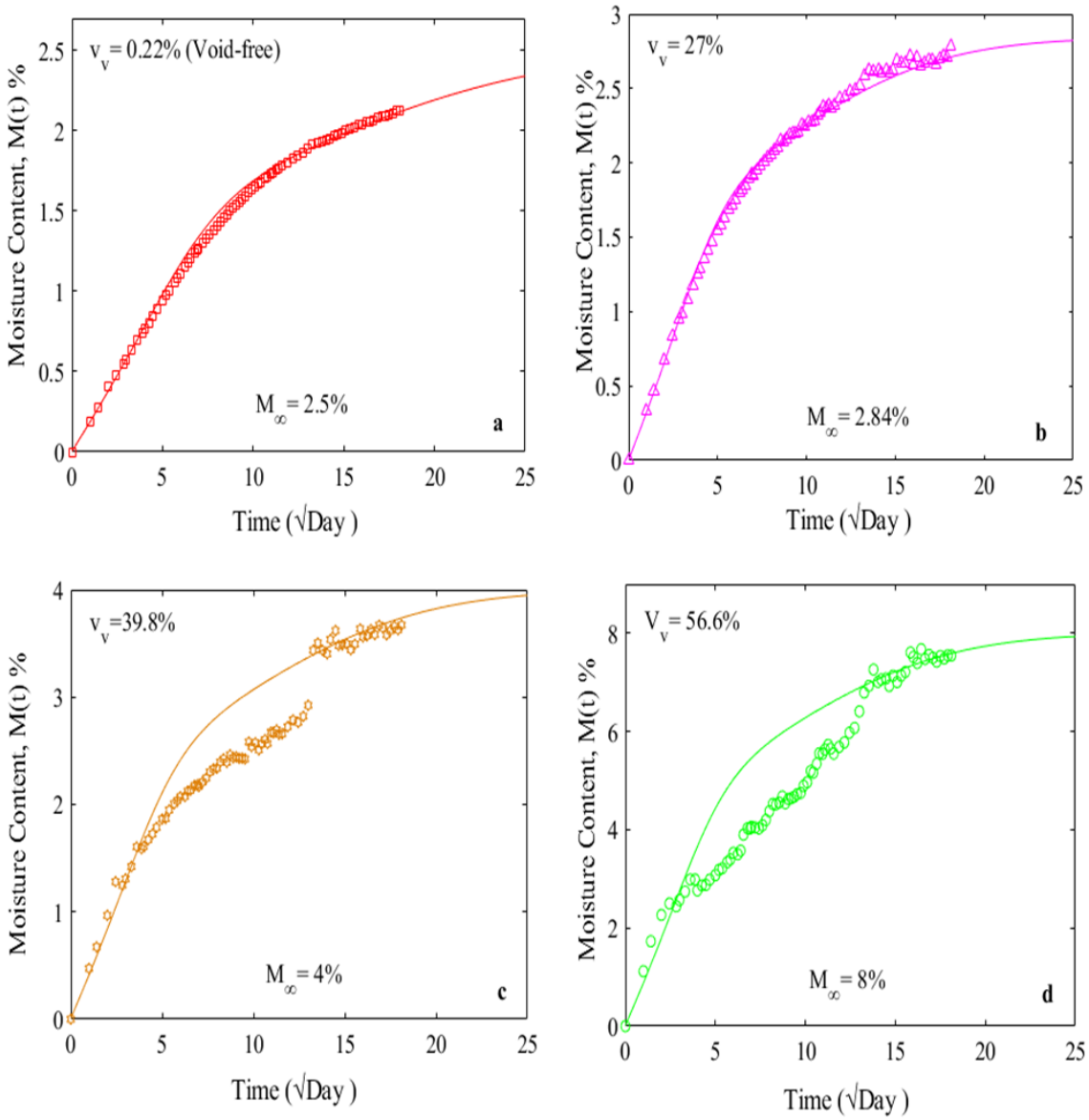

Figure 5.2 Langmuir model predictions and experimental moisture uptake results. a) void-free epoxy specimen, b) medium void content epoxy specimen, c) high void content specimen, and d) high void content (average data from 54.1 and 59.1%) specimen.

For the void-free specimens, Fig. 5.2a, the Langmuir model displays an almost perfect fit to the experimental data. This fit is much closer than the one from Fickian model shown in Fig. 5.1. The Langmuir model for specimens with void content 27% similarly displays a good fit, see Fig. 5.2b. For the specimen with 39% void content, Fig. 5.2c, the Langmuir model (M_∞ = 4%) fits the initial experimental data, although after about 170 days of immersion ($\sqrt{t} \approx 13$), a sudden discontinuity in the moisture content was observed. This may be due to a stepwise process where the diffusion front in the polymer reaches the region between two large, closely spaced voids as discussed for closed cell PVC foams by Earl and Shenoi (2004).

For the high void content specimens, The Langmuir model was fitted to the average moisture content data for 54.1 and 59.1% void contents. Fig 5.2d shows that the model fits the experimental data at short and long times. Between 20 and 200 days of immersion however, the Langmuir model overpredicts the moisture uptake. The reason for this deviation is not known, but may be related to a discontinuous water uptake mechanism due to large voids connected or separated by a thin wall as shown in Fig 4.1d. The microstructure of the high void content specimen, Fig. 4.1d, shows that several void cavities are connected and may form a channel. Channel flow may become interrupted by regions of solid polymer between voids which would temporarily slow down the water uptake.

Table 5.1 summarizes the saturation moisture contents, the diffusivity and the parameters β and α.

Table 5.1 Langmuir model parameters.

Specimen	v_v %	M_∞ %	D (m^2/day) x 10^{-8}	α (1/day) x 10^{-3}	β (1/day) x 10^{-3}
Void-Free	0.22	2.5	7.74	2.9	2.0
Medium void	27	2.84	18.1	6.6	4.4
High void	39	4.0	19.0	5.5	3.7
High void	56.6	8.0	20.6	6.3	4.2

The diffusivity for the void-free specimen (D = 7.74 x10^{-8} m^2/day) may be compared to literature data. Li et al. (2009) examined epoxy resin (DEGBA-DDM) immersed in water at 45 °C and obtained a diffusivity D = 6.4 x10^{-8} m^2/day which is close to our results. Joliff et al. (2013) found D =13 x10^{-8} m^2/day for epoxy resin immersed in water at 70 °C, which exceeds our value but the water temperature is higher than ours. Springer (1981) presents graphs for the diffusivity of epoxy over a wide range of temperatures. At 40 ºC the diffusivity is D = 5.18 x10^{-8} m^2/day, similar to our results.

Table 5.1 summarizes the four fitting parameters D, M_∞, β, and α for the void-free, medium and high void-content specimens. The diffusivity D is almost three times as high for specimens with voids compared to the void-free specimen. The diffusivity for the highest void content specimens (v_v=56%) is similar to that for the 27% void content specimen. The results shown in Fig. 5.2d for the highest void content specimens, however, reveal that the Langmuir model is not a good descriptor of the moisture uptake for this specimen, and the definition of the diffusivity parameter becomes questionable.

5.3 Mass Balance Model for Saturated Moisture Content

The moisture content at saturation of the void containing polymer specimen was analyzed based on mass balance calculations. The saturated moisture content of the void containing specimens was calculated for two limiting cases, viz. no water in the voids and voids fully filled with water. The moisture content M(t) is defined as,

$$\mathrm{M(t)} = \frac{\mathrm{m_w(t)}}{m} \tag{5.4}$$

where $m_w(t)$ is the mass of absorbed water after immersion time t, and m is the mass of dry specimen. The saturation moisture content is defined by,

$$\mathrm{M_\infty} = \frac{\mathrm{m_{w\infty}}}{m} \tag{5.5}$$

where $m_{w\infty}$ is the mass of absorbed water in the specimen at saturation.

If we first assume that voids do not take up water, the mass of absorbed water at saturation is,

$$\mathrm{m_{w\infty}} = \mathrm{V_r}\ \rho_r\ \mathrm{M_{r\infty}} \tag{5.6}$$

where ρ_r is the density of dry resin, V_r is the volume of solid polymer in the specimen, and $\mathrm{M_{r\infty}}$ is the saturation moisture content of the void-free resin. The mass of the dry resin is,

$$\mathrm{m} = V_r \rho_r \tag{5.7}$$

After substituting Eqs. (5.6) and (5.7) in (5.5),

$$\mathrm{M_\infty} = \frac{\mathrm{V_r}\ \rho_r\ \mathrm{M_{r\infty}}}{\mathrm{V_r}\ \rho_r} = \mathrm{M_{r\infty}} \tag{5.8}$$

Equation (5.8) shows that for this case (empty voids) the saturated moisture content is equal to that of the void-free resin.

The water absorption results, shown in Fig. (4.7) (Chapter 4), however show the saturation moisture content is quite strongly influenced by voids. As the other extreme we assume, at saturation that the voids become filled with water. At saturation, the moisture content M_∞ is:

$$M_\infty = \frac{V_r\,\rho_r\,M_{r\infty} + V_v\,\rho_w}{V_r\,\rho_r} \tag{5.9}$$

where V_v is the total volume of voids, and ρ_w is the density of water.

This expression M_∞ may be simplified to,

$$M_\infty = M_{r\infty} + \frac{V_v\,\rho_w}{V_r\,\rho_r} \tag{5.10}$$

The total volume of the void containing polymer V is defined by,

$$V = V_r + V_v \tag{5.11}$$

Hence V_r is given by,

$$V_r = V - V_v \tag{5.12}$$

Void content (void volume fraction) is given by,

$$v_v = \frac{V_v}{V} \tag{5.13}$$

By substituting (5.12) and (5.13) into (5.10), we obtain,

$$M_\infty = M_{r\infty} + \frac{v_v}{1-v_v} \cdot \frac{\rho_w}{\rho_r} \tag{5.14}$$

The mass balance analysis provides limits on the saturated moisture content, M_∞, of the void containing polymer as,

$$M_{r\infty} \leq M_\infty \leq M_{r\infty} + \frac{v_v}{1-v_v} \cdot \frac{\rho_w}{\rho_r} \tag{5.15}$$

where $M_{r\infty}$ is the saturation moisture content of the void-free resin, v_v is the void content, ρ_w is the density of water, ρ_r is the density of dry void-free resin.

The epoxy resin saturation moisture content $M_{r\infty}$ is 2.5% (Table 5.1). The mass balance analysis (Eq. (5.15)) predictions and the experiment results are listed in Table 5.2. The experimental results show that the void containing specimens absorb more water than the neat resin. The mass balance model predicts moisture contents of the void containing specimens up to 116 %. The experimental data shows that the specimens with voids absorb more water than the void-free, but the results in Table 5.2 show that the upper bound estimate representing voids fully filled by water is far from the actual data. To determine the degree of the void filling, the excess water absorption was considered. The results in Table 5.2 show that only about 6-8 % of the available void volume is occupied by water.

Our mass balance analysis results may be compared to the mass balance results by Humeau et al. (2015) for neat epoxy resin and glass fiber/epoxy composite specimens immersed in water under a range of hydrostatic pressures. They prepared void–free neat epoxy resin specimens (v_v = 0%), hand laid-up glass fiber/epoxy composite specimens (v_v= 4-6 %), and infused glass fiber/epoxy composite specimen (v_v = 0.5%). The void filling ratio for the hand laid-up composite specimens (v_v = 4-6 %) by Humeau et al. (2015) was 8% under atmospheric pressure (1 bar). This result is in agreement with ours. This ratio increased up to 60% with increasing hydrostatic pressure in the hand laid-up composite specimens. For

the infused composite specimens with a small void content, the void filling ratio was around 7% and did not depend on the hydrostatic pressure.

Table 5.2 Mass balance analysis results.

v_v %	Mass Balance Bounds, %		Experimental M_∞, %	% Void Filling
27	2.5	34.4	2.84	8.26
40	2.5	60.0	4	6.67
57	2.5	116	8	7.02

5.4 Micromechanics Predictions of Diffusivity

The micromechanics analysis outlined by Pal (2007) for the prediction of diffusivity explained in Section 2.7.2 was applied. According to the Maxwell model, the diffusivity for the void containing specimens can be expressed as follows,

$$\frac{D}{D_r} = 1 + 3\left(\frac{D_a - D_r}{D_a + 2D_r}\right)v_v \tag{5.16}$$

where D_r is resin moisture diffusivity, and v_v is the volume fraction of the voids. The voids are assumed to be filled by air. Hence D_a is the air diffusivity.

Cussler (2009) provides the air diffusivity D_a = 2.44 m^2/day. The resin moisture diffusivity (void-free) is obtained from our experimental data $D_r = 7.74 \times 10^{-8}$ m^2/day as listed in Table 4.9 in Section 4.6.1. The moisture diffusivity of air is several orders greater than the moisture diffusivity of the resin ($D_a >> D_r$), Eq. (5.16) can then be simplified as follows,

$$\frac{D}{D_r} = 1 + 3v_v \tag{5.17}$$

Figure 5.3 shows the diffusivity over a range of void contents from 0 to 60 % determined from Eq. (5.16) and our experimental data. The moisture diffusivity shows overall good agreement with the Maxwell model.

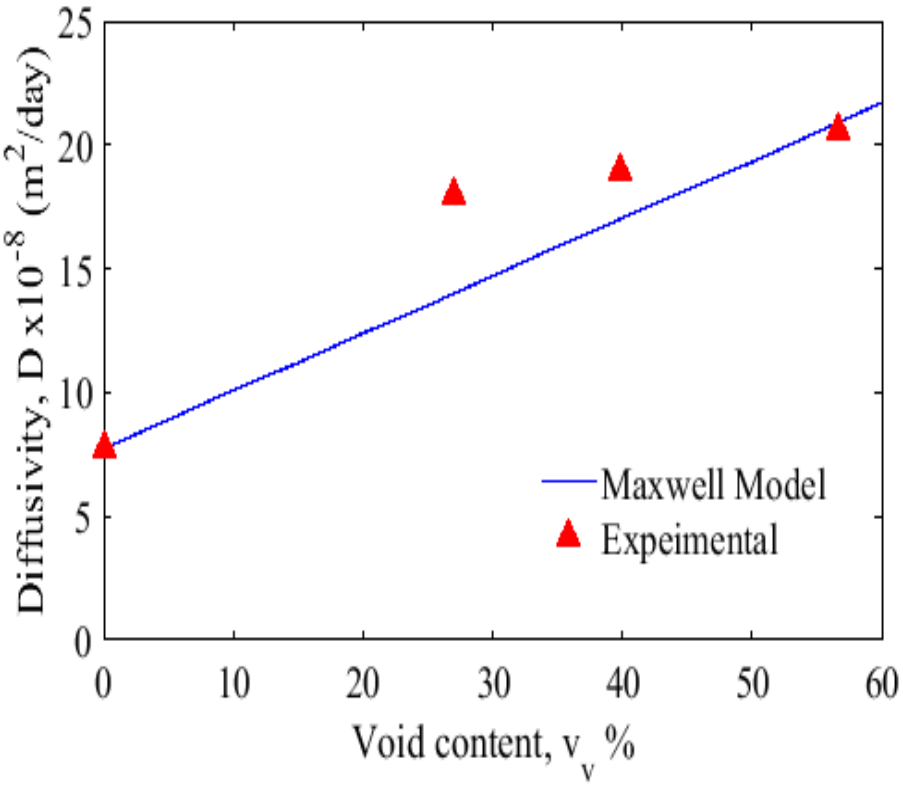

Figure 5.3 Diffusivity by Maxwell model and experimental results.

6 STATE OF WATER UP-TAKE AND SWELLING RESULT

The state of absorbed water for void-free and void containing epoxy was examined by DSC analysis. As discussed in Chapter 2, the sorbed water may broadly be divided into free water and bound water. The bound water may further be divided into freezable bound water and non-freezable bound water. DSC test were conducted on water-aged specimens with a large range of void contents as explained in Section 3.6.4.

6.1 DSC Analysis of Wet Specimens

Table 6.1 summarizes the DSC test program where void content, number of test specimens, and immersion time of the small DSC specimens are provided.

Table 6.1 DSC Test Matrix "F", "M" and "H" represents void-free, medium and high void content.

Void Content %	Designation	Number of tests	Immersion time (days)/ no of Specimens
0	SPF-3	1	0
2.47	SPF-2	2	7/1, 15 /1
26.6	SPM-7	2	7/1, 15/1
41.7	SPH-6a	2	7/2, 15/1
55.9	SPH-7a	1	15/1

The DSC cycles include cool-down from room temperature (RT) to -80 °C, and then heating to RT. The DSC analysis was first done on a dry void-free specimen SPF-3 (Table 6.1). Figure 6.1 shows the DSC data collected during the cooling and heating cycles. Neither the cooling curve, Fig. 6.1a, nor the heating curve Fig. 6.1b indicate any transition (as expected).

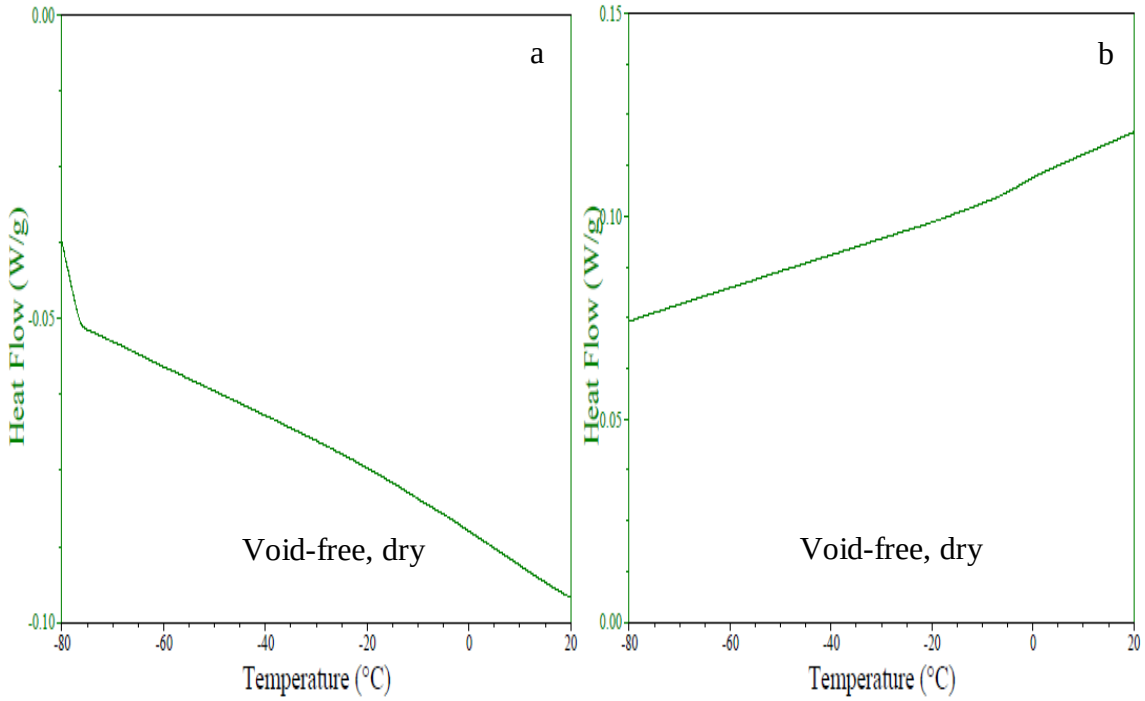

Figure 6.1 DSC curves for dry void-free specimen SPF-3, v_v= 0 %. a) cooling, b) heating.

DSC tests were then performed on a saturated void-free specimen (SPF-2 v_v=2.47%), a medium void content specimen (SPM-7, v_v= 26.6%), and two high void content specimens (SPH-6a, v_v= 41.7 % and SPH-7a, v_v= 55.8 %).

Figure 6.2 shows DSC curves for the void-free sample (SPF-2). The cooling and heating curves do not reveal any transitions. The small amount of absorbed water (2.5%) by this specimen is considered as non-freezable bound water, Eq. (2.6), see Section 2.6.4. Nakamura et al. (1983) found that their PpHS specimens required a moisture content of 9.2% before DSC analysis revealed a water transition.

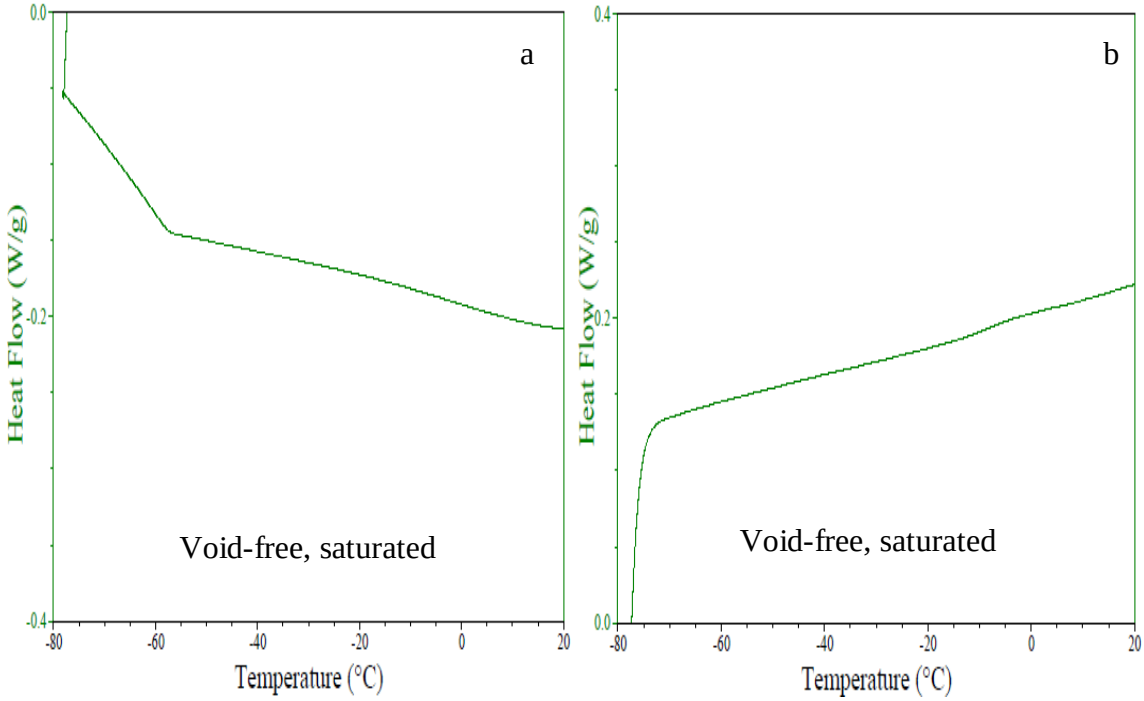

Figure 6.2 DSC curves for water aged void-free specimen SPF-2, v_v= 2.47 %. a) cooling, b) heating.

Figure 6.3 shows the DSC curves for a medium void content sample (SPM-7, v_v=26.6%) after 7 and 15 days of immersion. After 7 days of immersion, the cooling and heating curves (Figs. 6.3a and b) do not show any transition. After 15 days of immersion, however, three exothermic peaks are observed in the cooling curve (Fig. 6.3c) at temperatures of -19.5, -25.6 and -37.2 °C. The two first peaks are attributed to free water because the temperatures are close to the free water peak, see Fig. 2.11 (Section 2.6.3). The peak at -37.2 °C (Fig. 6.3c) is attributed to bound water (freezable bound water), see Fig. 2.11 (Section 2.6.3). During the heating cycle, Fig. 6.3d, an endothermic peak is observed at 0.43 °C. This peak is attributed to melting of the freezable free and bound water. Although the medium void content specimen absorbs relatively a small amount of water (2.85 %, Table 5.2 (Section 5.3), mass balance calculations. (Table 5.2) indicates that about 8% of the void volume contains water, which may be registered as free water.

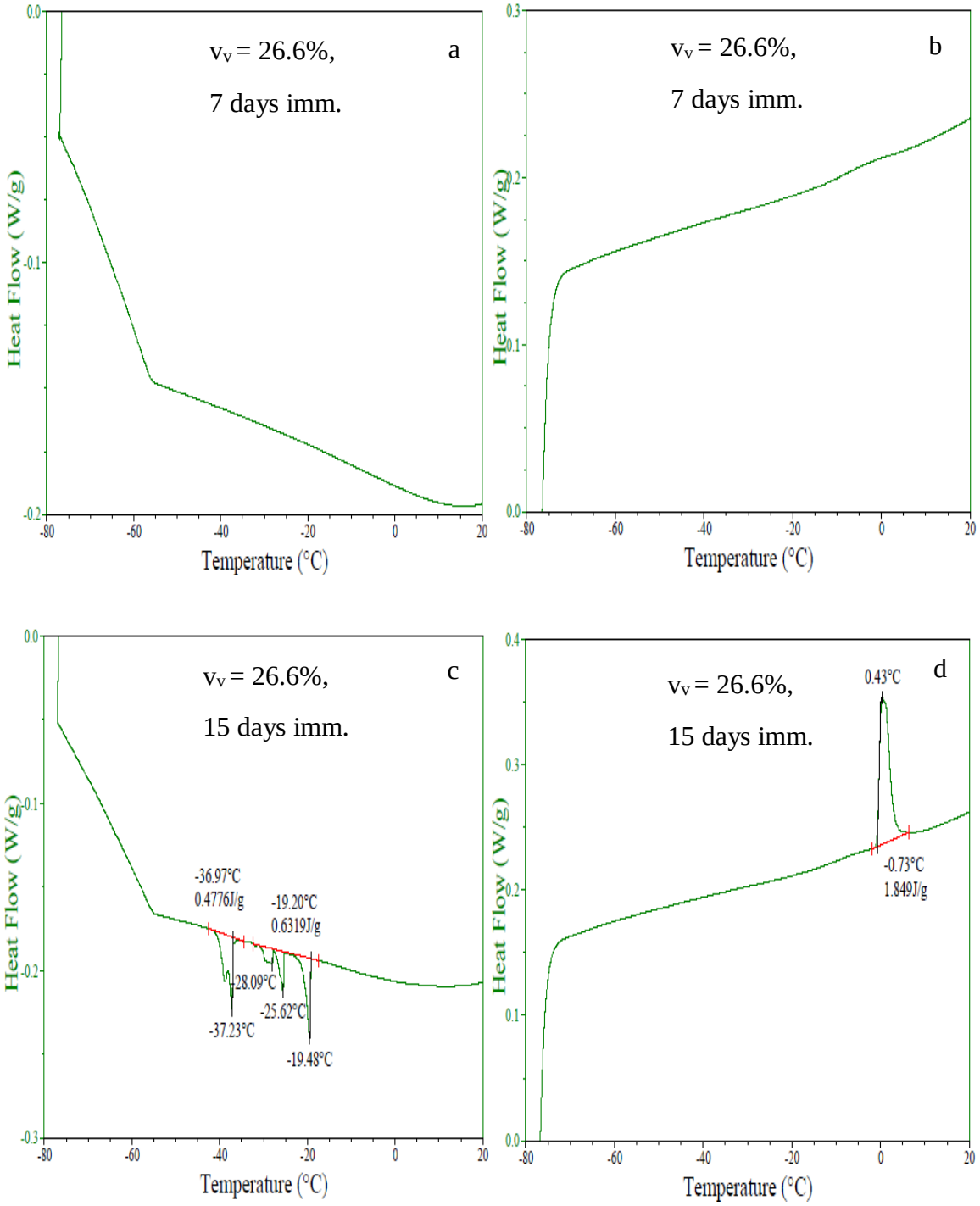

Figure 6.3 DSC curves for medium void content water aged specimen SPM-7, v_v= 26.6%. a) cooling and b) heating curves after 7 days of immersion, c) cooling and d) heating curves after 15 days of immersion.

DSC results for high void content specimen (SPH-6a, v_v=41.6%) are shown in Fig. 6.4. In the cooling curve for 7 days immersion (Fig. 6.4a), a sharp exothermic peak is observed at -18 ℃ which is attributed to free water. During heating of the specimen, Fig. 6.4b, an endothermic peak is observed at 0.56 ℃ which is due to melting of the freezable water (free and bound water). For specimen immersed for 15 days, two exothermic peaks are observed in the cooling curve (Fig. 6.4c), one at -18.8 ℃ corresponding to free water and one at -38.9 ℃ (Fig. 6.4c) due to bound water. The heating cycle, Fig. 6.4d reveals a large endothermic peak at 0.81 ℃ attributed to melting of free and freezable bound water.

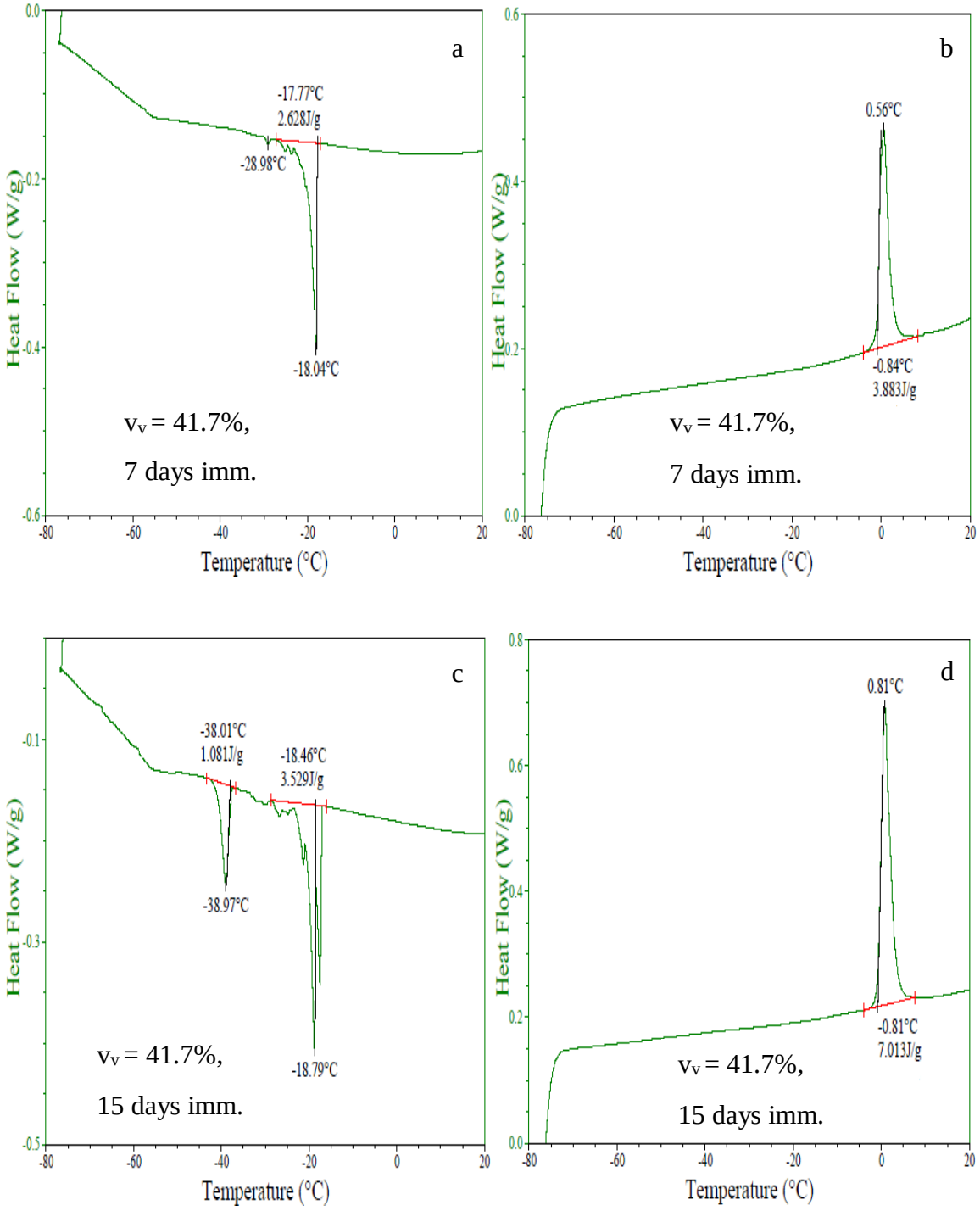

Figure 6.4 DSC curves for high void content specimen SPH-6a, v_v= 41.7%. a) cooling and b) heating curves after 7 days of immersion, c) cooling and d) heating curves after 15 days of immersion.

Figure 6.5 shows the DSC results for another high void content specimen (SPH-7a, v_v=55.6 %) after immersion for 15 days. A peak is observed in the cooling curve, Fig. 6.5a, at -16.7 °C which is attributed to free water. A small exothermic peak is observed at -38.5 °C which is attributed to freezable bound water. The heating curve, Fig. 6.5b, reveals an endothermic peak at 1.45 °C corresponding to melting of free and freezable bound water. Notice that the results for the 55.6 % void content specimen shown in Fig. 6.5 are similar to those for the 41.6 % void content specimen shown in Fig. 6.4c, d although, the enthalphies are larger for the 55.6% void content specimen.

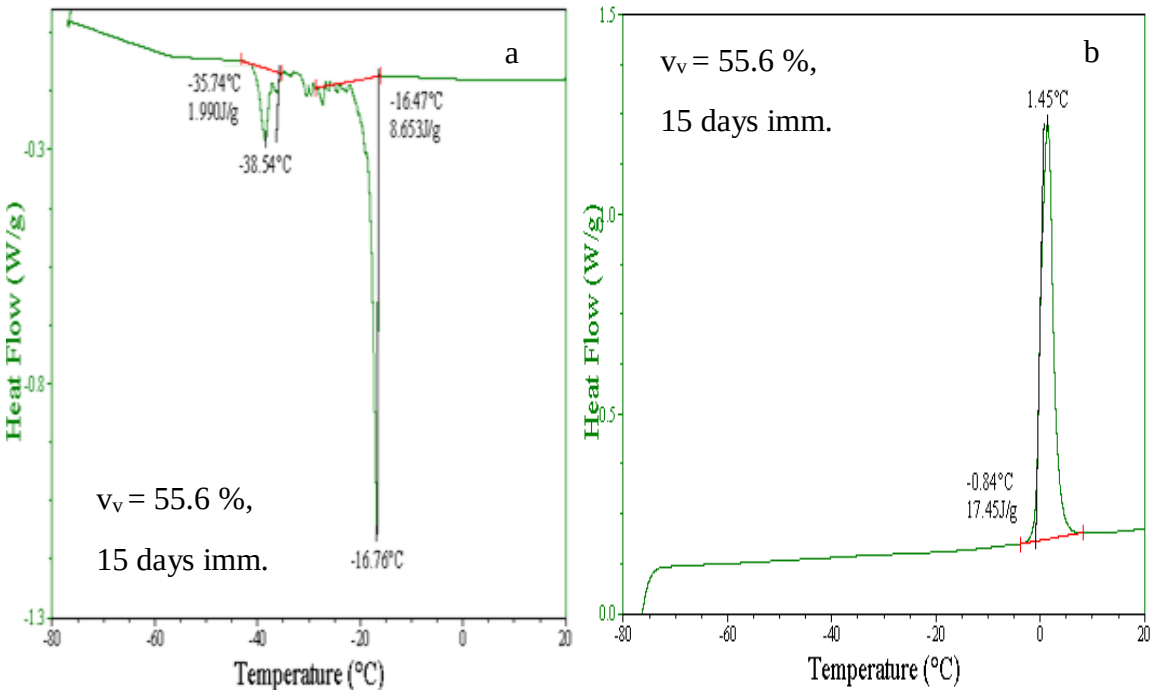

Figure 6.5 DSC curves for high void content epoxy specimen SPH-7a (v_v= 55.6%) after 15 days of immersion. a) cooling, b) heating.

6.2 Free and Bound Water Contents

Table 6.2 summarizes the transition temperatures and enthalphies for the test specimens obtained from the DSC tests as shown in Figs. 6.1 - 6.5. The free water transition temperature was consistent, around -18.0 °C. Similarly, the bound water transition temperatures were all around -38 °C and the freezable water transition at about 0.7 °C. The measured enthalphies corresponding to the three peaks, Fig. 2.11 (Section 2.6.3), are listed in Table 6.2.

Table 6.2 DSC analysis results summary (transition temperature (T) and enthalphy (Q)). "F", "M", and "H" represent void-free, medium, and high void contents. The enthalphies Q_f, Q_b, and Q_{fz} are defined in Eqs. (2.6) - (2.9).

Void Content, v_v %	Designation	Free water		Bound water		Freezable water	
		T °C	Q_f J/kg	T °C	Q_b J/kg	T °C	Q_{fz} J/kg
0.22	SPF-2 (7 days)	N/A	N/A	N/A	N/A	N/A	N/A
26.6	SPM-7 (7 days)	N/A	N/A	N/A	N/A	N/A	N/A
	(15 days)	-19.5	0.63	-37.0	0.47	0.43	1.85
41.7	SPH-6a (7 days)	-18.0	2.63	N/A	N/A	0.56	3.88
	(15 days)	-18.8	3.53	-38.9	1.08	0.81	7.01
55.8	SPH-7a (15 days)	-16.7	8.7	-38.5	1.99	1.45	17.45

Notice that enthalphies for the high void content specimen are higher after 15 days of immersion than after 7 days due to the increased moisture content.

The contents of freezable and non-freezable bound water determined from the enthalphies using Eqs. (2.5 - 2.8) are listed in Table 6.3 and shown graphically in Fig. 6.6. As pointed

out earlier, the void-free specimen contains only non-freezable bound water. With increasing void content, the content of freezable water increases, while the content of non-freezable bound water remains fairly constant.

Table 6.3 Freezable and non-freezable bound water contents.

Specimen	v_v, %	M_t %	Freezable water content %	Non-freezable bound water content %
SPF-2	0.22	2.5	0	2.5
SPM-7	26.6	2.85	0.63	2.22
SPH-6a	41.7	4	2.4	1.6
SPH-7a	55.6	8	6	2

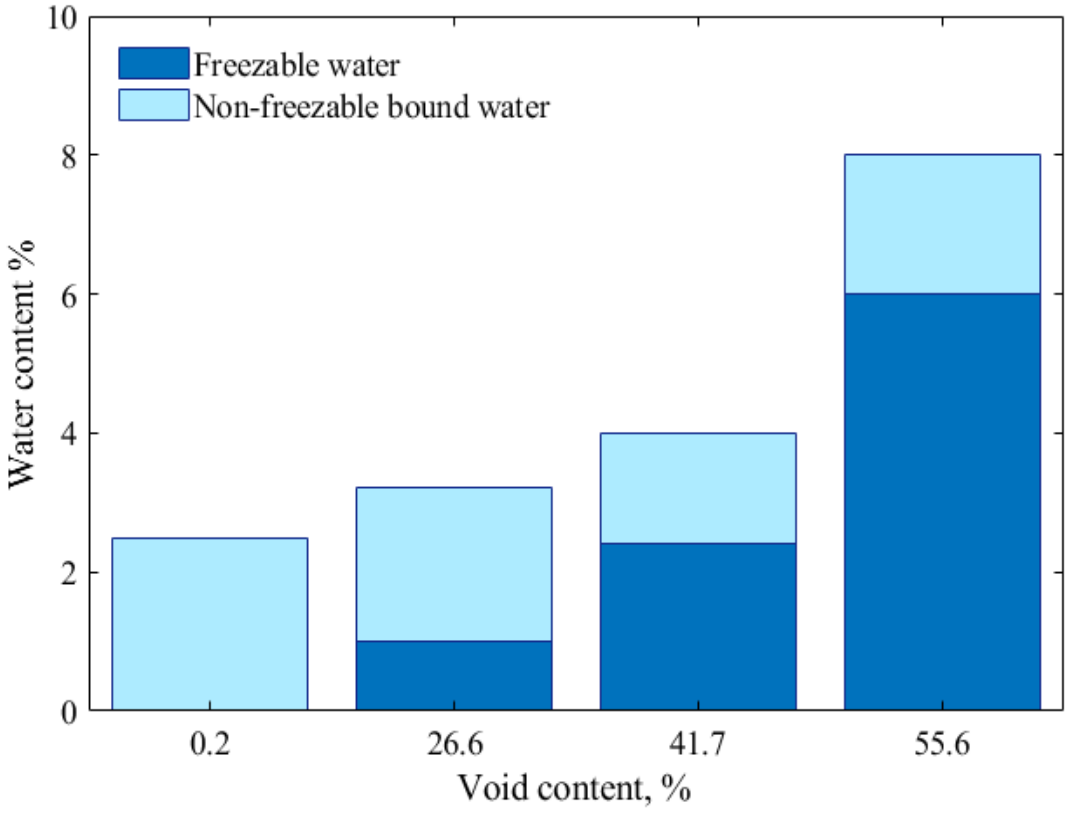

Figure 6.6 Contents of freezable water and non-freezable bound water for void-free, medium void and high void content epoxy specimens.

The freezable water consists of free water and freezable bound water (see Eqs. 2.5 - 2.8). Table 6.4 lists the contents of free and freezable bound water. It may be noted that the content of the freezable water is slightly greater than the sum of the contents of free water and freezable bound water which may be due inaccuracy in the determination of the enthalphy of freezable bound water (Q_b) which is a small area in the DSC cooling curve. The contents of free and freezable bound water are plotted in Fig. 6.7. The content of free water increases quite strongly with void content, and so does the content of freezable bound water.

Table 6.4 Free and freezable bound water contents.

Specimen,	v_v%	M_t %	Q_f	Q_b	Free water content %	Freezable bound water content %
SPF-2	0.22	2.5	0	0	0	0
SPM-7	26.6	2.85	0.63	0.47	0.27	0.21
SPH-6a	41.7	4	3.53	1.08	1.61	0.50
SPH-7a	55.6	8	8.7	1.99	4.0	0.91

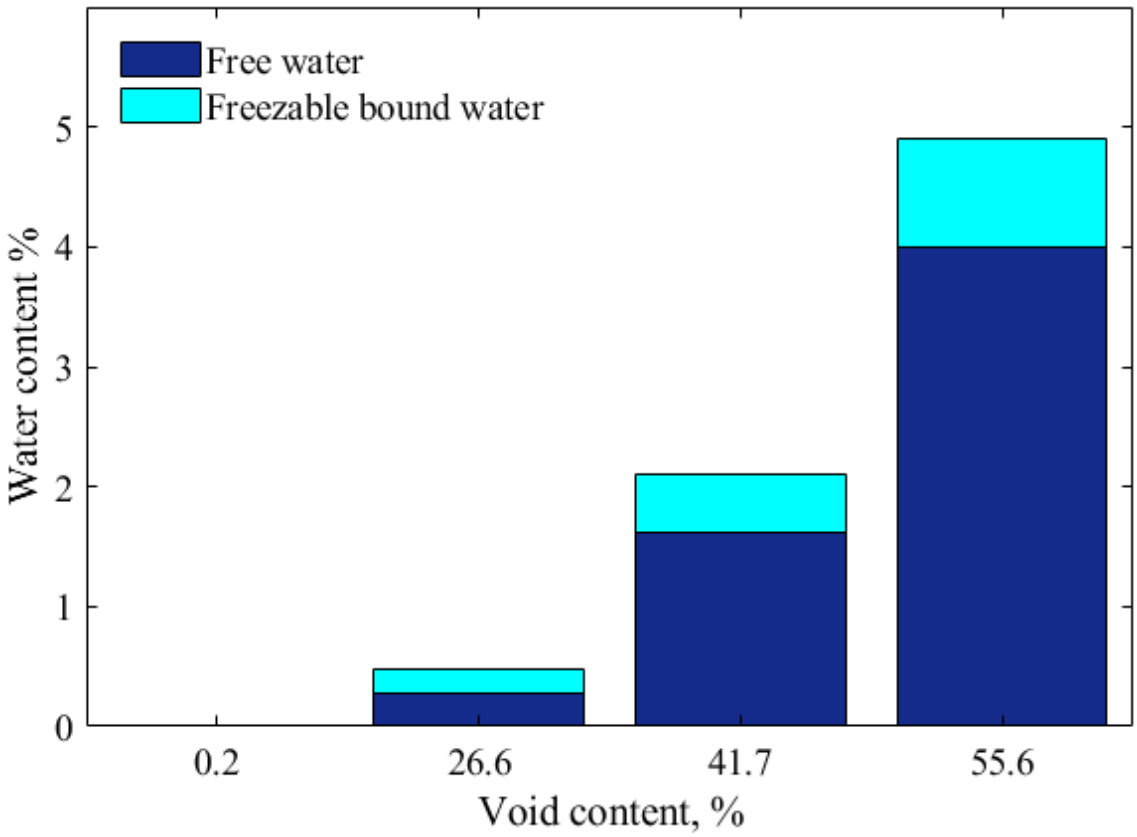

Figure 6.7 Contents of free water and freezable bound water for void-free, medium void and high void content epoxy specimens.

6.3 Swelling Results

Figure 6.8 shows the moisture swelling strain ($\Delta V/V_0$) plotted vs. void content. The highest swelling is observed for the void-free specimen. The medium and high void content specimens show much less swelling than the void-free specimen. The swelling strain may be quantified by the moisture expansion coefficient and the amount of moisture absorbed (moisture content). It is noted that the moisture swelling of the polymer is expected to follow the same micromechanics equations as the thermal expansion coefficient (α). For a particulate system, the thermal expansion coefficient can be calculated using Turner formula, Turner (1946) and Nielsen (1967), as follows,

$$\alpha = \frac{\frac{\propto_1 W_1 E_1}{\rho_1} + \frac{\propto_2 W_2 E_2}{\rho_2}}{\frac{W_1 E_1}{\rho_1} + \frac{W_2 E_2}{\rho_2}} \tag{6.1}$$

where w is the weight fraction of the two constituents (air and polymer), E is Young's modulus, ρ is the density, and the subscript 1 for the matrix and 2 for the inclusion. The inclusions in this case (voids) have no stiffness ($E_2 = 0$). Substitution of $E_2 = 0$ in Eq. (6.1) yields $\alpha = \alpha_1$. Hence, by this analogy, the voids should not influence the moisture expansion.

The resin chemistry was shown to remain consistent for the void-free and void containing specimens, see Section 4.4. It therefore seems reasonable to assume that the material properties of the various void containing specimens, such as the moisture expansion coefficient of the epoxy matrix should be independent of void content. Hence, any difference in swelling should be related to differences in the moisture content of the epoxy matrix.

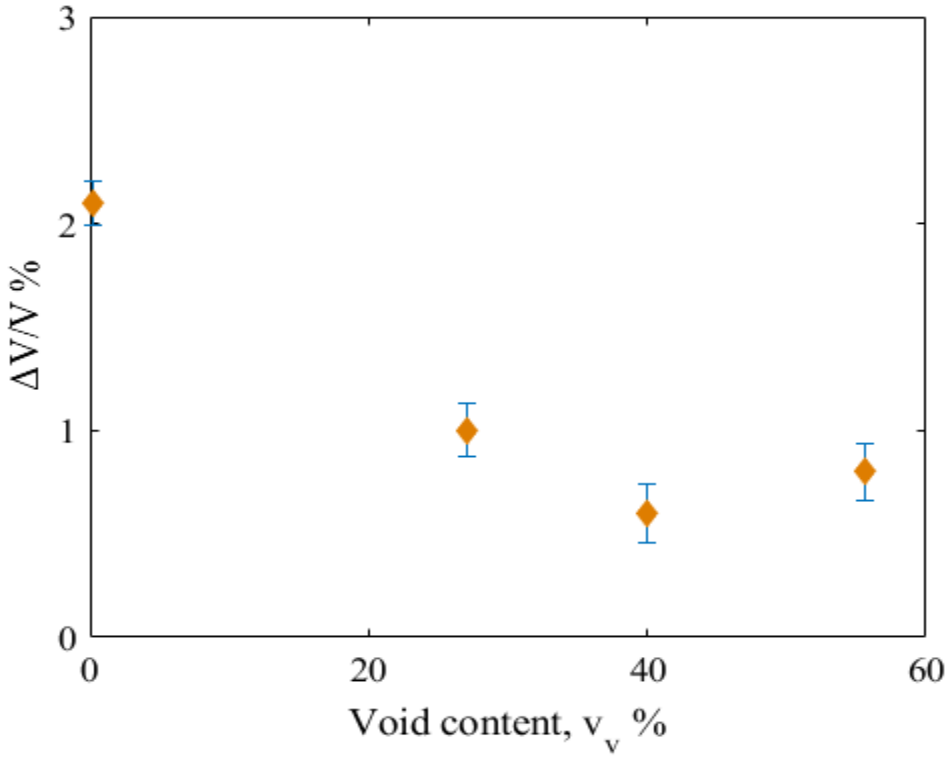

Figure 6.8 Swelling strain vs. void content for epoxy specimens.

As an upper limit, it would be argued that the swelling is bound by the potential volume increase due to the additional volume of sorbed water $\Delta V_w/V_0$. This ratio was determined for the specimens by converting the mass of absorbed water to volume. The added mass of sorbed water is given by,

$$m_w = \mathrm{M(t)m_0} \tag{6.2}$$

where M(t) is the moisture content and m_0 is the mass of dry specimen.

The added volume due to the sorbed water becomes,

$$\Delta V_w/V_0 = \frac{\mathrm{M(t)\ m_0}}{\rho_w\, V_0} \tag{6.3}$$

Here ρ_w is the water density, $\rho_w = 1\ \mathrm{g/cm^3}$.

Table 6.5 lists the potential volume increase due to absorbed water $\Delta V_w/V_0$ and moisture swelling ($\Delta V/V_0$) for the void-free, medium void and high void content specimens. The results are shown graphically in Figure 6.9. The results in Fig. 6.9 show that the moisture swelling of the void-free specimen is close to the upper bound ($\Delta V_w/V_0$). Adamson (1980) similarly found that the swelling of moisture saturated 3501-6 epoxy specimens is below the volume due to added water. He attributed the reduction in swelling to water contained in the free volume, this water will not contribute to swelling.

Table 6.5 Potential volume increase due to water absorbed $\Delta V_w/V_0$ and moisture swelling ($\Delta V/V_0$) for void-free, medium void and high void content specimens. "F", "M", and "H" represent void-free, medium, and high void contents.

v_v %	($\Delta V_w/V_0$) %	Swelling ($\Delta V/V_0$) %
0.22 (F)	2.6	2.1 ± 0.11
27 (M)	2.28	1.0 ± 0.13
40 (H)	2.65	0.6 ± 0.14
56.6 (H)	4.0	0.8 ± 0.135

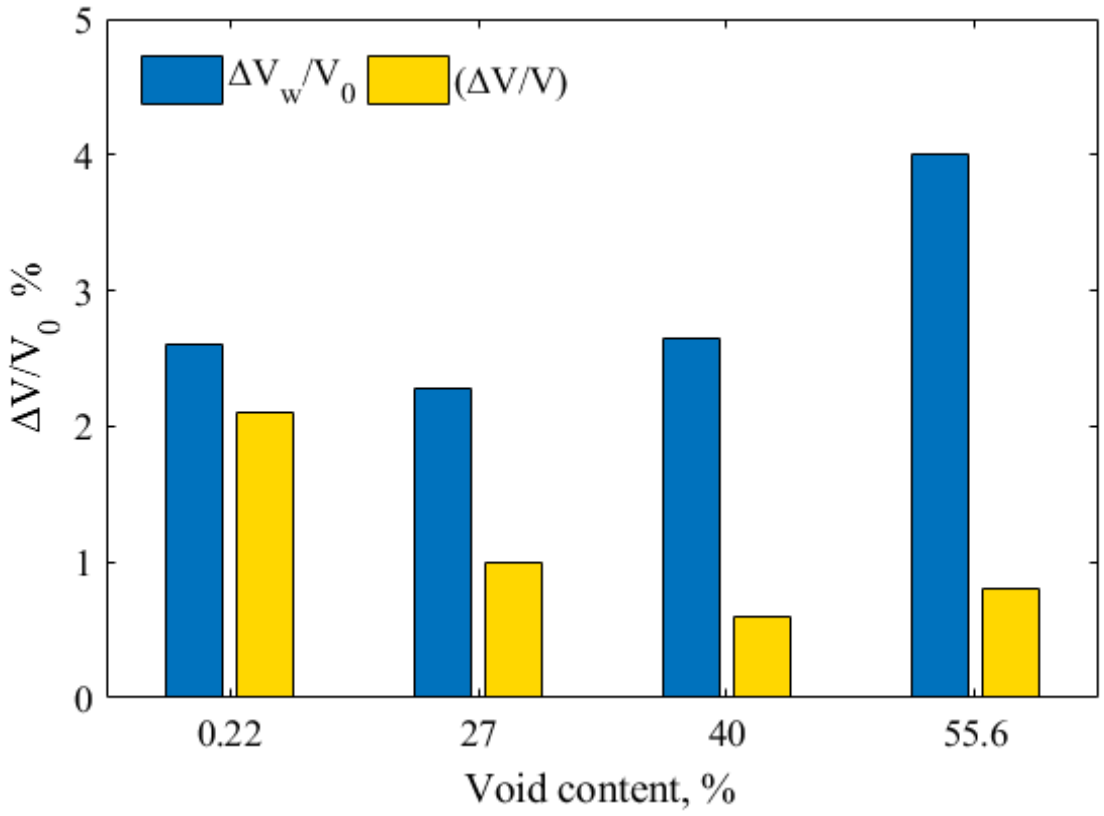

Figure 6.9 Moisture swelling and potential volume increase due to moisture absorbed for void-free, medium void and high void content epoxy specimens.

For the specimens with voids considered here, Fig. 6.9, it is observed that the moisture swelling $\Delta V/V_0$ falls significantly below potential volume that increases due to added water ($\Delta V_w/V_0$). Although the water absorption increase with void content, this is not converted to swelling. The results in Fig. 6.9 show that the total water content has no direct influence on the moisture swelling of the polymer. A more reasonable assumption would be to assume that the non-freezable bound water is responsible for swelling since it causes breakage of hydrogen bonds in the polymer network and expand the volume. Figure 6.10 shows the swelling ratio plotted vs. the ratio of non-freezable water content to the total water content. Considering the scatter and uncertainties associated with the data points, the

results seem to support the hypothesis that the non-freezable bound water is responsible for swelling.

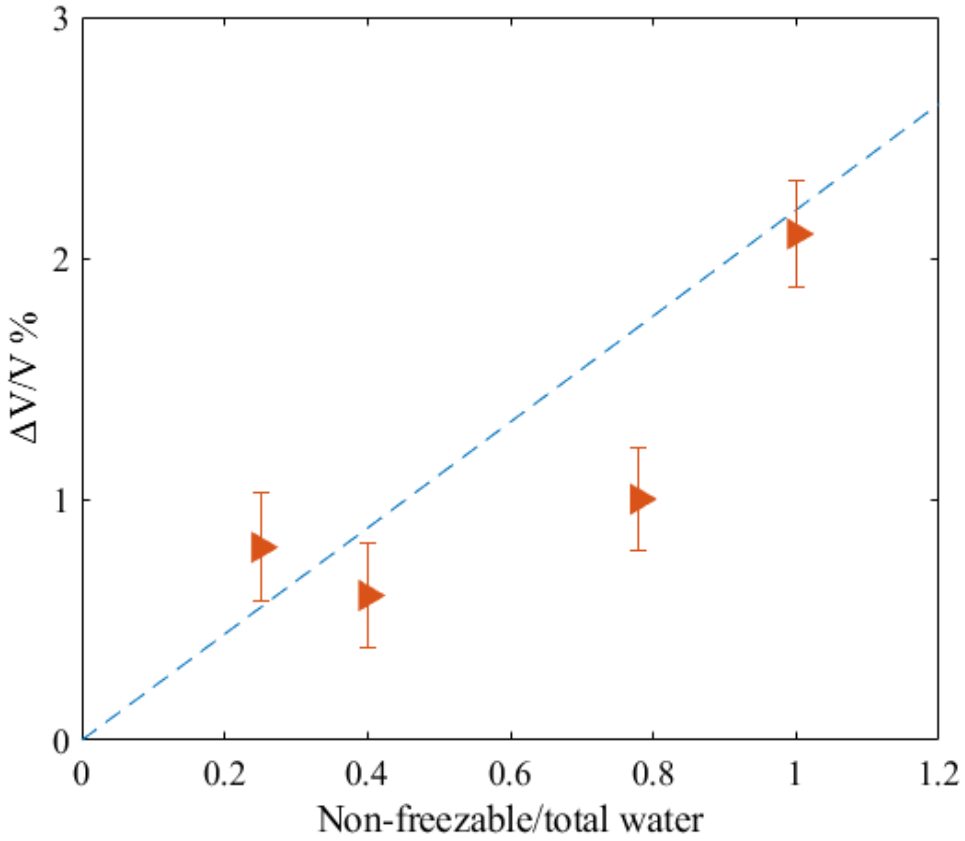

Figure 6.10 Moisture swelling ΔV/V % vs. non-freezable water/total water for epoxy specimens.

7 CONCLUSIONS

In this thesis, we have examined the influence of voids on the water absorption by an epoxy polymer. Methods to fabricate void-free and void containing epoxy specimens have been developed using chemicals added to achieve controlled foaming. The specimens were characterized experimentally in terms of void structure, void content and water absorption. DSC and DMA tests on dry void-free and void containing specimens verified that T_g for the void containing specimens is close to T_g for the void-free specimens indicating consistent chemistry of the epoxy network. Void structure (void shape and size), and void content were characterized using microscopy of sectioned specimens, ImageJ analysis and density measurements. Microscopic analysis indicate that the voids are close to spherical in shape and isolated, except for specimens with very high void contents, where regions of connected voids are observed. In all cases the void size was much less than the thickness of the moisture aging specimens. The moisture uptake increases with increased void content, both in terms of rate and saturation moisture content. Moisture uptake was analyzed using the classical Fickian analysis and a two-phase Langmuir model. The Langmuir model gives good fits to the experimental moisture uptake data for void-free and medium void content specimens. The water uptake results for the high void content specimens showed discontinuous water uptake response. The water uptake mechanism did not obey the Langmuir model which may be due to closely spaced large voids which was shown in the specimen microstructure. Connected voids are likely to change the moisture

transport mechanism. The diffusivity of the specimens with void contents from 0 to 56 % agreed reasonably with the Maxwell inclusion model.

The influence of voids on the state of absorbed water in epoxy has been examined by DSC analysis of water aged specimens. The sorbed water is categorized as free water and bound water. The bound water is further partitioned into freezable and non-freezable water. DSC analysis of moisture aged specimens was conducted from RT to -80 °C followed by a heating cycle back to RT. For the void-free specimens, the DSC analysis showed that all the sorbed water is bound non-freezable water. For the medium and high void contents specimens, both free and bound water transitions were found in the DSC curves. A mass balance analysis indicates that at saturation only a small fraction of the void volume (6 - 8%) is filled with water, and that this fraction is quite independent of the void content. The content of free water was calculated from enthalphies determined from the DSC analysis. The content of non-freezable water (bound water) is large in the void-free specimens and decreased with increasing void content. Moisture induced swelling decreased with increasing void content. The swelling was attributed to the content of non-freezable bound water as determined by DSC analysis.

8 REFERENCES

Adamson, M.J., 1980. Thermal expansion and swelling of cured epoxy resin used in graphite/epoxy composite materials. Journal of materials science, 15(7), pp.1736-1745.

Aklonis, J.J. and MacKnight, W.J., Introduction to Polymer Viscoelasticity. 1983. A Wiley-Interscience Publication: New York.

ASTM D5229, 1998, Standard test method for moisture absorption properties and equilibrium conditioning of polymer matrix composite materials, ASTM International, West Conshohocken.

ASTM D792-08, 2008, "Standard test method for density and specific gravity (relative density) of plastics by displacement", West Conshohocken, PA, ASTM International.

ASTM D2734-09, Standard test methods for void content of reinforced plastics, ASTM International, West Conshohocken, PA, 2009.

Bonniau, P. and Bunsell, A.R., 1981. A comparative study of water absorption theories applied to glass epoxy composites. Journal of Composite Materials, 15(3), pp. 272-293.

Budd, P.M., McKeown, N.B. and Fritsch, D., 2005. Free volume and intrinsic microporosity in polymers. Journal of Materials Chemistry, 15(20), pp.1977-1986.

Carnachan, R.J., Bokhari, M., Przyborski, S.A. and Cameron, N.R., 2006. Tailoring the morphology of emulsion-templated porous polymers. Soft Matter, 2(7), pp.608-616.

Carter, H.G. and Kibler, K.G., 1978. Langmuir-type model for anomalous moisture diffusion in composite resins. Journal of Composite Materials, 12(2), pp. 118-131.

Crank, J., 1979. The Mathematics of Diffusion. 2nd ed. Clarendon Press, Oxford.

De'Nève, B. and Shanahan, M.E.R., 1993. Water absorption by an epoxy resin and its effect on the mechanical properties and infra-red spectra. Polymer, 34(24), pp.5099-5105.

Earl, J.S. and Shenoi, R.A., 2004. Determination of the moisture uptake mechanism in closed cell polymeric structural foam during hygrothermal exposure. Journal of Composite Materials, 38(15), pp. 1345-1365.

Foreman, J., 1997. Dynamic mechanical analysis of polymers. American Laboratory, 29, pp. 21-24.

Glaskova, T.I., Guedes, R.M., Morais, J.J. and Aniskevich, A.N., 2007. A comparative analysis of moisture transport models as applied to an epoxy binder. Mechanics of Composite Materials, 43(4), pp.377-388.

González, M.G., Cabanelas, J.C. and Baselga, J., 2012. Applications of FTIR on epoxy resins-identification, monitoring the curing process, phase separation and water uptake. In Infrared Spectroscopy-Materials Science, Engineering and Technology, 13, (T. Theophile ed.), pp. 262-284.

Grave, C., McEwan, I. and Pethrick, R.A., 1998. Influence of stoichiometric ratio on water absorption in epoxy resins. Journal of Applied Polymer Science, 69(12), pp.2369-2376.

Hatakeyama, T., Nakamura, K. and Hatakeyama, H., 1988. Determination of bound water content in polymers by DTA, DSC and TG. Thermochimica Acta, 123, pp. 153-161.

Hatakeyama, H. and Hatakeyama, T., 1998. Interaction between water and hydrophilic polymers. Thermochimica Acta, 308(1-2), pp. 3-22.

Hatakeyama, T. and Quinn, F.X., 1999. Thermal Analysis: Fundamentals and Applications to Polymer Science, 2nd edition, John Wiley & Sons, Chichester.

He, Y. and Fan, X., 2007, May. In-situ characterization of moisture absorption and desorption in a thin BT core substrate. In Electronic Components and Technology Conference, 2007. ECTC'07. Proceedings. 57th (pp. 1375-1383). IEEE, Reno, Nevada, USA.

Hilliard, J.E., 1968. Measurement of volume in volume", Quantitative Microscopy (PP. 45-76), DeHoff, R.T. and Rhines, F.N., eds., McGraw-Hill, New York.

Hodge, R.M., Edward, G.H. and Simon, G.P., 1996. Water absorption and states of water in semicrystalline poly (vinyl alcohol) films. Polymer, 37(8), pp. 1371-1376.

Hughes, S.W., 2005. Archimedes revisited: a faster, better, cheaper method of accurately measuring the volume of small objects. Physics Education, 40(5), p. 468.

Humeau, C., Davies, P. and Jacquemin, F., 2016. Moisture diffusion under hydrostatic pressure in composites. Materials & Design, 96, pp. 90-98.

Jordan, J.L., Foley, J.R. and Siviour, C.R., 2008. Mechanical properties of Epon 826/DEA epoxy. Mechanics of Time-Dependent Materials, 12(3), pp. 249-272.

Kuo, C.Y. and Frost, J.D., 1996. Uniformity evaluation of cohesionless specimens using digital image analysis. Journal of Geotechnical Engineering, 122(5), pp. 390-396.

Li, L., Yu, Y., Wu, Q., Zhan, G. and Li, S., 2009. Effect of chemical structure on the water sorption of amine-cured epoxy resins. Corrosion Science, 51(12), pp. 3000-3006.

Li, X. and Weitsman, Y.J., 2004. Sea-water effects on foam-cored composite sandwich lay-ups. Composites Part B: Engineering, 35(6), pp. 451-459.

Little, J.E., Yuan, X. and Jones, M.I., 2012. Characterisation of voids in fibre reinforced composite materials. NDT & E International, 46, pp. 122-127.

López, C.C., Lefebvre, X., Brusselle-Dupend, N., Klopffer, M.H., Cangémi, L., Castagnet, S. and Grandidier, J.C., 2016. Effect of porosity and hydrostatic pressure on water absorption in a semicrystalline fluoropolymer. Journal of Materials Science, 51(8), pp. 3750-3761.

Maggana, C. and Pissis, P., 1999. Water sorption and diffusion studies in an epoxy resin system. Journal of Polymer Science Part B: Polymer Physics, 37(11), pp. 1165-1182.

Manfredi, L.B., Fraga, A.N. and Vázquez, A., 2006. Influence of the network structure and void content on hygrothermal stability of resol resin modified with epoxy–amine. Journal of Applied Polymer Science, 102(1), pp. 588-597.

Maxwell, I.D. and Pethrick, R.A., 1983. Dielectric studies of water in epoxy resins. Journal of Applied Polymer Science, 28(7), pp. 2363-2379.

Mendoza, F. and Lu, R., 2015. Basics of Image Analysis. In: Park, B. and Lu, R. (eds) Hyperspectral Imaging Technology in Food and Agriculture. Food Engineering Series. Springer, New York.

Mutlur, S., 2004. Thermal analysis of composites using DSC. In "Advanced topics in characterization of composites", (ed. M. Kessler), Victoria, Trafford Publishing, pp.11-33.

Nakamura, K., Hatakeyama, T. and Hatakeyama, H., 1981. Studies on bound water of cellulose by differential scanning calorimetry. Textile Research Journal, 51(9), pp. 607-613.

Nakamura, K., Hatakeyama, T. and Hatakeyama, H., 1983. Relationship between hydrogen bonding and bound water in polyhydroxystyrene derivatives. Polymer, 24(7), pp.871-876.

Nielsen, L.E., 1967. Mechanical properties of particulate-filled systems. Journal of Composite Materials, 1(1), pp. 100-119.

Nogueira, P., Ramirez, C., Torres, A., Abad, M.J., Cano, J., Lopez, J., López-Bueno, I. and Barral, L., 2001. Effect of water sorption on the structure and mechanical properties of an epoxy resin system. Journal of Applied Polymer Science, 80(1), pp. 71-80.

Osswald, T.A. and Menges, G., 2003. Materials Science of Polymers for Engineers. Carl Hanser Verlag, Munich.

Paciornik, S. and d'Almeida, J.R.M., 2009. Measurement of void content and distribution in composite materials through digital microscopy. Journal of Composite Materials, 43(2), pp. 101-112.

Pal, R., 2007. New models for thermal conductivity of particulate composites. Journal of Reinforced Plastics and Composites, 26(7), pp. 643-651.

Papthanasiou, T.D. and Guell, D.C. (Eds.), 1997. Flow-induced Alignment in Composite Materials. Elsevier, Cambridge

Perrin, F.X., Nguyen, M.H. and Vernet, J.L., 2009. Water transport in epoxy–aliphatic amine networks–Influence of curing cycles. European Polymer Journal, 45(5), pp. 1524-1534.

Ping, Z.H., Nguyen, Q.T., Chen, S.M., Zhou, J.Q. and Ding, Y.D., 2001. States of water in different hydrophilic polymers - DSC and FTIR studies. Polymer, 42(20), pp. 8461-8467.

Poapongsakorn P, Carlsson LA. Fracture toughness of closed-cell PVC foam: Effects of loading configuration and cell size. Composite Structures. 2013 Aug 31; 102:1-8.

Rasband, W.S., 1997. ImageJ software. National Institutes of Health: Bethesda, MD, USA.

Rusch, K.C., 1968. Time-temperature superposition and relaxational behavior in polymeric glasses. Journal of Macromolecular Science, Part B: Physics, 2(2), pp.179-204.

Santulli, C., Gil, R.G., Long, A.C. and Clifford, M.J., 2002. Void content measurements in commingled E-glass/polypropylene composites using image analysis from optical micrographs. Science and Engineering of Composite Materials, 10(2), pp. 77-90.

Springer, G.S. (ed.) 1981, Environmental Effects on Composite Materials, Technomic Publishing Co. Inc. Westport.

Stefani, P.M., Barchi, A.T., Sabugal, J. and Vazquez, A., 2003. Characterization of epoxy foams. Journal of Applied Polymer Science, 90(11), pp. 2992-2996.

Thomason, J.L., 1995a. The interface region in glass fibre-reinforced epoxy resin composites: 1. Sample preparation, void content and interfacial strength. Composites, 26(7), pp. 467-475.

Thomason, J.L., 1995b. The interface region in glass fibre-reinforced epoxy resin composites: 2. Water absorption, voids and the interface. Composites, 26(7), pp. 477-485.

Trautschold, O.C., 2016. A literature review on the study of moisture in polymers (No. LA-UR--16-23708). Los Alamos National Lab. (LANL), Los Alamos, NM.

Turner, P. S. 1946. Thermal expansion stresses in reinforced plastics. Journal Research of NBS, 37, pp. 239-250.

Vesely, D., 2008. Diffusion of liquids in polymers. International Materials Reviews, 53(5), pp. 299-315.

Wang, Y., 2013. Low Density Epoxy Foams for Wind Energy Application, Master Thesis, University of Houston, 2013.

Weitsman, Y.J., 2012. Fluid Sorption Data and Modeling. In Fluid Effects in Polymers and Polymeric Composites (pp. 31-68). Mechanical Engineering Series. Springer, Boston.

Wright, P., Fu, X., Sinclair, I. and Spearing, S.M., 2008. Ultra high resolution computed tomography of damage in notched carbon fiber—epoxy composites. Journal of Composite Materials, 42(19), pp.1993-2002.

Xiao, G.Z., Delamar, M. and Shanahan, M.E.R., 1997. Irreversible interactions between water and DGEBA/DDA epoxy resin during hygrothermal aging. Journal of Applied Polymer Science, 65(3), pp. 449-458.

Young, R.J. and Lovell, P.A., 2011. Introduction to Polymers. 3rd edition, CRC press, Boca Raton.

Zhou, J. and Lucas, J.P., 1999. Hygrothermal effects of epoxy resin. Part I: the nature of water in epoxy. Polymer, 40(20), pp. 5505-5512.

Zhou, J. and Lucas, J.P., 1999. Hygrothermal effects of epoxy resin. Part II: variations of glass transition temperature. Polymer, 40(20), pp. 5513-5522.